

# Deliberate Planning of 3D Bin Packing on Packing Configuration Trees

Journal Title  
XX(X):1-??  
©The Author(s) 2016  
Reprints and permission:  
sagepub.co.uk/journalsPermissions.nav  
DOI: 10.1177/ToBeAssigned  
www.sagepub.com/

SAGE

Hang Zhao<sup>2</sup>, Juzhan Xu<sup>3</sup>, Kexiong Yu<sup>1</sup>, Ruizhen Hu<sup>3</sup>, Chenyang Zhu<sup>1</sup>, and Kai Xu<sup>1</sup>

## Abstract

Online 3D Bin Packing Problem (3D-BPP) has widespread applications in industrial automation and has aroused enthusiastic research interest recently. Existing methods usually solve the problem with limited resolution of spatial discretization, and/or cannot deal with complex practical constraints well. We propose to enhance the practical applicability of online 3D-BPP via learning on a novel hierarchical representation—packing configuration tree (PCT). PCT is a full-fledged description of the state and action space of bin packing which can support packing policy learning based on deep reinforcement learning (DRL). The size of the packing action space is proportional to the number of leaf nodes, i.e., candidate placements, making the DRL model easy to train and well-performing even with continuous solution space. We further discover the potential of PCT as tree-based planners in deliberately solving packing problems of industrial significance, including large-scale packing and different variations of BPP setting. A recursive packing method is proposed to decompose large-scale packing into smaller sub-trees while a spatial ensemble mechanism integrates local solutions into a global one. For different BPP variations with additional decision variables, such as lookahead, buffering, and offline packing, we propose a unified planning framework enabling out-of-the-box problem solving based on a pre-trained PCT model. Extensive evaluations demonstrate that our method outperforms existing online BPP baselines and is versatile in incorporating various practical constraints. Driven by PCT, the planning process excels across large-scale problems and diverse problem variations, with performance improving as the problem scales up and the decision variables grow. To verify our method, we develop a real-world packing robot for industrial warehousing, with careful designs accounting for constrained placement and transportation stability. Our packing robot operates reliably and efficiently on unprotected pallets at 10 seconds per box. It achieves averagely 19 boxes per pallet with 57.4% space utilization for relatively large-size boxes.

## Keywords

Bin Packing Problem, Robot Packing, Reinforcement Learning, Industrial Embodied Intelligence

## 1 Introduction

As one of the most classic combinatorial optimization problems, the 3D bin packing problem usually refers to packing a set of cuboid-shaped items  $i \in \mathcal{I}$ , with sizes  $s_i^x, s_i^y, s_i^z$  along  $x, y, z$  axes, respectively, into the maximum space utilization of bin  $C$  with sizes  $S^x, S^y, S^z$ , in an axis-aligned fashion. Traditional 3D-BPP assumes that all the items to be packed are known a priori (Martello et al. 2000), which is also called *offline* BPP. The problem is known to be strongly NP-hard (De Castro Silva et al. 2003). However, in many real-world application scenarios, e.g., logistics or warehousing (Wang and Hauser 2019a), the upcoming items cannot be fully observed; only the current item to be packed is observable. Packing items without the knowledge of all upcoming items is referred to as *online* BPP (Seiden 2002).

Due to its obvious practical usefulness, online 3D-BPP has received increasing attention recently. Given the limited knowledge, the problem cannot be solved by usual search-based methods. Different from offline 3D-BPP where the items can be placed in an arbitrary order, online BPP must place items following their coming order, which imposes additional constraints. Online 3D-BPP is usually solved with either heuristic methods (Ha et al. 2017) or learning-based ones (Zhao et al. 2021), with complementary pros and cons.

Heuristic methods are generally not limited by the size of the action space, but they find difficulties in handling complex practical constraints such as packing stability. Learning-based approaches typically outperform heuristic methods, particularly under complex constraints. However, their convergence is challenging when the action space is large, which limits their applicability due to the restricted resolution of spatial discretization (Zhao et al. 2021).

We propose to enhance learning-based online 3D-BPP towards practical applicability through learning with a novel hierarchical representation—*packing configuration tree (PCT)*. PCT is a dynamically growing tree where the internal nodes describe the space configurations of packed items and leaf nodes the packable placements of the current item. PCT is a full-fledged description of the state and action space of bin packing which can support packing policy learning based on deep reinforcement learning (DRL).

<sup>1</sup>National University of Defense Technology, China

<sup>2</sup>Wuhan University, China

<sup>3</sup>Shenzhen University, China

## Corresponding author:

Kai Xu, National University of Defense Technology, China.

Email: kevin.kai.xu@gmail.com

We extract state features from PCT using graph attention networks (Velickovic et al. 2018) which encode the spatial relations of all configuration nodes. The state feature is input into the actor and critic networks of the DRL model. The actor network, designed based on a pointer mechanism, weighs the leaf nodes and outputs the final placement.

During training, PCT grows under the guidance of heuristics such as *corner point* (Martello et al. 2000), *extreme point* (Crainic et al. 2008), and *empty maximal space* (Ha et al. 2017). Although PCT is expanded with heuristic rules, confining the solution space to what the heuristics could explore, our DRL model learns a discriminant fitness function (the actor network) for the candidate placements, resulting in an effective and robust packing policy exceeding the heuristic methods. Furthermore, the size of the packing action space is proportional to the number of leaf nodes, making the DRL model easy to train and well-performing even with continuous solution space.

PCT was published in ICLR 2022 (Zhao et al. 2022a), which is the first learning-based method that successfully solves online 3D-BPP with continuous solution space and achieves strong performance. We believe that its potential extends beyond regular online packing and further discover its capability as tree-based planners to deliberately solve packing problems of industrial significance, including large-scale packing and different variations of BPP setting. We propose *recursive packing* to decompose the tree structure of large-scale online 3D-BPP as smaller sub-trees to individually solve them. The obtained local solutions are then integrated into a global one through an effective *spatial ensemble* method. In addition to online packing, PCT’s enhanced representation of packing constraints and flexible action space can be extended to other mainstream BPP settings, such as lookahead, buffering, and offline packing. We propose a unified planning framework enabling out-of-the-box problem solving based on a pre-trained PCT model.

We have established a real-world packing robot in an industrial warehouse, carefully designed to meet *constrained placement* (Choset et al. 2005) and *transportation stability* (Hof et al. 2005) requirements. Unlike laboratory setups with protective container walls (Yang et al. 2021a; Xu et al. 2023), our system operates under industrial standards with boxes (items) directly placed onto unprotected pallets. Even minor robot-object collisions during placement can destabilize the static stack, and dynamic transportation by Automated Guided Vehicles (AGVs) or human workers may further challenge the stack’s stability. To satisfy constrained placement, our system incorporates a modular end-effector capable of actively adjusting its shape to maximize gripping force while minimizing collision risk. To ensure transportation stability, we perform physics-based verification via test-time simulation to account for real-world uncertainties. Each placement is evaluated under multiple sets of disturbances, with the simulation accelerated by GPU-based batch parallelism (Makovychuk et al. 2021). Combined with an asynchronous decision-making pipeline that overlaps decision time with robot execution, our packing robot operates efficiently and reliably on unprotected pallets in industrial settings, with a cycle time of 10 seconds per box and averagely 19 boxes per pallet (57.4% space utilization

for relatively large-size boxes). A video showcasing our dynamic packing process is provided at this [URL](#).

Our works make the following contributions (those which are newly introduced in this paper are marked with the bullet symbol of ‘\*’):

- We propose a full-fledged tree description for online 3D-BPP, which further enables efficient packing policy learning based on DRL.
- PCT is the first learning-based method that successfully solves online 3D-BPP with continuous solution space, achieving state-of-the-art performance.
- \* We propose recursive packing to decompose large-scale packing problems and spatial ensemble to integrate local solutions into a global one.
- \* We propose a unified planning framework to solve different BPP variations out of the box, based on a pre-trained PCT model without fine-tuning.
- \* We develop an industrial packing robot that meets constrained placement and transportation stability, operating reliably on standard unprotected pallets.

## 2 Related Work

### 2.1 3D Bin Packing Problems

Given a single bin  $C$  and a set of items  $\mathcal{I}$ , the objective of the 3D bin packing problem (3D-BPP) (Martello et al. 2000) is to maximize the space utilization. Its basic constraints can be formulated as follows:

$$\text{Maximize: } \sum_{i=1}^N v_i \quad v_i = s_i^x \cdot s_i^y \cdot s_i^z, \quad (1)$$

$$\text{Subject to: } p_i^d + s_i^d \leq p_j^d + S^d(1 - e_{ij}^d), \quad \forall i \neq j, \quad (2)$$

$$0 \leq p_i^d \leq S^d - s_i^d, \quad (3)$$

where  $p_i$  denotes the Front-Left-Bottom (FLB) coordinate of item  $i \in \mathcal{I}$ , and  $N$  is the total number of items after packing. The variable  $d \in \{x, y, z\}$  represents the axis. If item  $i$  is placed before item  $j$  along axis  $d$ , the value of  $e_{ij}^d$  is 1; otherwise, it is 0. Equations 2 and 3 represent the non-overlapping constraint and containment constraint (Martello et al. 2000), respectively.

The early interest in 3D-BPP mainly focused on its offline setting. Offline 3D-BPP assumes that all items are known a priori and can be placed in an arbitrary order. Martello et al. (2000) first solved this problem with an exact branch-and-bound approach. Limited by the exponential worst-case complexity of exact approaches, lots of heuristic and meta-heuristic algorithms are proposed to get an approximate solution quickly, such as guided local search (Faroe et al. 2003), tabu search (Crainic et al. 2009), and hybrid genetic algorithm (Kang et al. 2012). Hu et al. (2017) decompose the offline 3D-BPP into packing order decisions and online placement decisions. This two-step fashion is widely accepted and followed by Duan et al. (2019), Hu et al. (2020), and Zhang et al. (2021).

Although offline 3D-BPP has been well studied, their search-based approaches cannot be directly transferred to the online setting. As a result, many heuristic methods have been proposed. For reasons of simplicity and good performance, the deep-bottom-left (DBL) heuristic (Karabulut and

Inceoglu 2004) has long been the preferred choice. Ha et al. (2017) sort the empty spaces with this DBL order and place the item into the first fit one. Wang and Hauser (2019b) propose a Heightmap-Minimization method to minimize the volume increase of the packed items as observed from the loading direction. Hu et al. (2020) optimize the empty spaces available for the packing future with a Maximize-Accessible-Convex-Space method.

## 2.2 Learning-based Online Packing

The heuristic methods are intuitive to implement and can be easily applied to various scenarios. However, the price of good flexibility is that these methods perform mediocrely, especially for online 3D-BPP with specific constraints. Designing new heuristics for specific classes of 3D-BPP is heavy work since this problem has an NP-hard solution space where many situations need to be premeditated manually by trial and error. Substantial domain knowledge is also necessary to ensure safety and reliability. To automatically generate a policy that works well on specified online 3D-BPP, Verma et al. (2020) and Zhao et al. (2021) employ DRL to solve this problem, however, their methods only work in discrete and small coordinate spaces. Despite their limitations, these works are soon followed for logistics robot implementation (Hong et al. 2020; Yang et al. 2021b; Zhao et al. 2022b). Referring to Hu et al. (2017), Zhang et al. (2021) adopt a online placement policy for offline packing needs. All these learning-based methods work in a grid world with limited discretization accuracy, which reduces their practical applicability. PCT overcomes these limitations by explicitly storing the necessary packing configuration information in a structured packing representation and using graph neural networks to capture spatial relationships. This allows PCT to better represent the packing state, enhancing the performance of DRL.

PCT is the first learning-based method to successfully solve online 3D-BPP in continuous solution space. Its core idea is to identify a finite set of candidates from the continuous domain and use DRL to determine the best solution. This candidate-based packing mechanism has been widely adopted in subsequent work. Yuan et al. (2023) and Pan et al. (2023b) optimize PCT policies from specific perspectives about performance variance and lower bounds. TAP-NET++ (Xu et al. 2023) extends this approach by simultaneously calculating the attention between multiple candidates and multiple items to address buffering packing (Puche and Lee 2022). Zhao et al. (2023) theoretically prove the local optimality of limited candidates for packing irregularly shaped items, using DRL to find the global solution. SDF-Pack (Pan et al. 2023a) focuses on finding a currently greedy, compact solution, but the most compact placement at a given moment is not necessarily optimal for the entire packing sequence.

## 2.3 Practical Constraints of Industrial Packing

The majority of literature on 3D-BPP (Martello et al. 2000) focuses primarily on basic non-overlapping constraint 2 and containment constraint 3. Failing to consider essential real-world constraints, such as stability (Ramos et al. 2016), these algorithms have limited industrial applicability.

Zhao et al. (2022b) propose a fast quasi-static equilibrium estimation method tailored for DRL training and test their learned policies with real logistics boxes. A key limitation of their approach is the use of a heightmap (the upper frontier of packed items) state representation, similar to Zhang et al. (2021), which overlooks the underlying constraints between packed items. The lack of spatial information in this representation makes the problem a partially observable Markov Decision Process (POMDP) (Spaan 2012), which complicates DRL training and limits performance on more complex practical 3D-BPP instances involving constraints like isle friendliness and load balancing (Gzara et al. 2020). PCT overcomes these limitations by explicitly storing the necessary packing configuration information in a tree structure and using graph attention networks (Velickovic et al. 2018) to capture spatial relationships. This allows PCT to better represent the packing state, thereby enhancing the performance of DRL.

Large-scale packing plays a critical role in production. For truck packing (Egeblad et al. 2007), hundreds of items must be packed online before long-distance transportation. However, DRL methods face challenges when applied to large-scale combinatorial optimization (CO) tasks (Kool et al. 2019; Qiu et al. 2022). On the one hand, exploring via trial and error struggles to collect sufficient learning samples in the enormous NP-hard space. On the other hand, long sequences of decision-making leads to learning instability (Sutton and Barto 2018). While recent studies demonstrate that graph-based neural solvers exhibit problem scale generalizability (Sun and Yang 2023), performance degradation is still observed due to test distribution mismatches (Yu et al. 2024). Leveraging the structured packing representation of PCT, we recursively decompose large-scale packing into smaller sub-trees and integrate local solutions into a global one using a spatial ensemble mechanism. This deliberate planning achieves state-of-the-art performance on large-scale packing, with performance continuing to improve as the the problem scales up.

In industrial applications, strictly online BPP (Seiden 2002) is not the only demand, and additional packing settings along with decision variables need to be considered. For example, lookahead packing (Grove 1995) allows for observing upcoming items in advance for enabling better placement of the current one. Buffering packing (Puche and Lee 2022) temporarily stores incoming items in a buffer, allowing the robot to select any one of them within reach. Offline packing (Martello et al. 2000; Demisse et al. 2012) receives complete item information from the central control system to schedule their arrival order. While various solvers have been proposed recently to address these settings, they typically rely on additional parameterized modules (Hu et al. 2017; Duan et al. 2019) to handle the extra constraints and decision variables, increasing training overhead and decreasing transferability. The advantages of PCT—better constraint representation and more flexible decision-making—can also benefit these settings. We induce these problems into distinct planning processes, where the constraints do not conflicts, allowing problems solved with a unified framework out of the box. Without fine-tuning requirement, this framework achieves consistency state-of-the-art performance across various BPP settings.



### 3 Method

We begin by introducing our learning-based packing solver, PCT, and demonstrating its enhanced representation of packing constraints and flexible action space in Section 3.1. In Section 3.2, we formalize PCT-based packing as a Markov Decision Process (MDP) for policy learning. Using pre-trained PCT models, we then perform deliberate planning to solve packing problems with industrial significance: large-scale packing and different variations of BPP setting. In Section 3.3, we present a recursive packing method to tackle large-scale challenges, along with a spatial ensemble mechanism to integrate local solutions into a global one. In Section 3.4, we introduce a unified planning framework that solves different BPP variations out of the box.

#### 3.1 Packing Configuration Tree

When a rectangular item  $n_t$  is added to a given packing with position  $(p_n^x, p_n^y, p_n^z)$  at time step  $t$ , it introduces a series of new candidate positions where future items can be accommodated, as illustrated in Figure 1. Combined with the axis-aligned orientation  $o \in \mathbf{O}$  for  $n_t$  based on existing positions, we get candidate placements (i.e. position and orientation). The packing process can be seen as a placement node being replaced by a packed item node, and new candidate placement nodes are generated as children. As the packing time step  $t$  goes on, these nodes are iteratively updated and a dynamic *packing configuration tree* is formed, denoted as  $\mathcal{T}$ . The internal node set  $\mathbf{B}_t \in \mathcal{T}_t$  represents the space configurations of packed items, and the leaf node set  $\mathbf{L}_t \in \mathcal{T}_t$  the packable candidate placements. During the packing, leaf nodes that are no longer feasible, e.g., covered by packed items, will be removed from  $\mathbf{L}_t$ . When there is no packable leaf node that makes  $n_t$  satisfy the constraints of placement, the packing episode ends. Without loss of generality, we stipulate a vertical top-down packing within a single bin (Wang and Hauser 2021).

Traditional 3D-BPP literature only cares about the remaining placements for accommodating the current item  $n_t$ , their packing policies can be written as  $\pi(\mathbf{L}_t|\mathbf{L}_t, n_t)$ . If we want to promote this problem for practical demands, 3D-BPP needs to satisfy more complex practical constraints which also act on  $\mathbf{B}_t$ . Taking packing stability for instance, a newly added item  $n_t$  has possibly force and torque effects on the whole item set  $\mathbf{B}_t$  (Ramos et al. 2016). The addition of  $n_t$  should make  $\mathbf{B}_t$  a stable spatial distribution so that more items can be added in the future. Therefore, our packing policy over  $\mathbf{L}_t$  is defined as  $\pi(\mathbf{L}_t|\mathcal{T}_t, n_t)$ , which means probabilities of selecting leaf nodes from  $\mathbf{L}_t$  given  $\mathcal{T}_t$  and  $n_t$ . For online packing, we hope to find the best leaf node selection policy to expand the PCT with more relaxed constraints so that more future items can be appended.

**Leaf Node Expansion** The performance of online 3D-BPP policies has a strong relationship with the choice of leaf node expansion schemes—which incrementally calculate new candidate placements introduced by the just placed item  $n_t$ . A good expansion scheme should reduce the number of solutions to be explored while not missing too many feasible packings. Meanwhile, polynomials computability is also expected. Designing such a scheme from scratch is non-trivial. Fortunately, several placement rules independent

from particular packing problems have been proposed, such as *Corner Point* (Martello et al. 2000), *Extreme Point* (Crainic et al. 2008), and *Empty Maximal Space* (Ha et al. 2017). We extend these schemes, which have proven to be accurate and efficient, to our PCT expansion. Their performance will be reported in Section 4.1.

**Tree Representation** Given the bin configuration  $\mathcal{T}_t$  and the current item  $n_t$ , the packing policy can be parameterized as  $\pi(\mathbf{L}_t|\mathcal{T}_t, n_t)$ . The tuple  $(\mathcal{T}_t, n_t)$  can be treated as a graph and encoded by Graph Neural Networks (GNNs) (Gori et al. 2005). Specifically, the PCT keeps growing with time step  $t$  and cannot be embedded by spectral-based approaches (Bruna et al. 2014) requiring fixed graph structure. We adopt non-spectral Graph Attention Networks (GATs) (Velickovic et al. 2018), which require no graph structure priori.

The raw space configuration nodes  $\mathbf{B}_t, \mathbf{L}_t, n_t$  are presented by descriptors in different formats. We use three independent node-wise Multi-Layer Perceptron (MLP) blocks to project these heterogeneous descriptors into the homogeneous node features:  $\hat{\mathbf{h}} = \{\phi_{\theta_B}(\mathbf{B}_t), \phi_{\theta_L}(\mathbf{L}_t), \phi_{\theta_n}(n_t)\} \in \mathbb{R}^{d_h \times N}$ ,  $d_h$  is the dimension of node feature and  $\phi_{\theta}$  is an MLP block with parameters  $\theta$ . The feature number  $N = |\mathbf{B}_t| + |\mathbf{L}_t| + 1$  is a variable. The GAT layer is used to transform  $\hat{\mathbf{h}}$  into high-level node features. The Scaled Dot-Product Attention (Vaswani et al. 2017) is applied to each node for calculating the relation weight of one node to another. These relation weights are normalized and used to compute the linear combination of features  $\hat{\mathbf{h}}$ . The feature of node  $i$  embedded by the GAT layer can be represented as:

$$\text{GAT}(\hat{h}_i) = W^O \sum_{j=1}^N \text{softmax} \left( \frac{(W^Q \hat{h}_i)^T W^K \hat{h}_j}{\sqrt{d_k}} \right) W^V \hat{h}_j, \quad (4)$$

where  $W^Q \in \mathbb{R}^{d_k \times d_h}$ ,  $W^K \in \mathbb{R}^{d_k \times d_h}$ ,  $W^V \in \mathbb{R}^{d_v \times d_h}$ , and  $W^O \in \mathbb{R}^{d_h \times d_v}$  are projection matrices.  $d_k$  and  $d_v$  are dimensions of projected features. The softmax operation normalizes the relation weight between node  $i$  and node  $j$ . The initial feature  $\hat{\mathbf{h}}$  is embedded by a GAT layer and the skip-connection operation (Vaswani et al. 2017) is followed to get the final output features  $\mathbf{h}$ :

$$\mathbf{h}' = \hat{\mathbf{h}} + \text{GAT}(\hat{\mathbf{h}}), \quad \mathbf{h} = \mathbf{h}' + \phi_{FF}(\mathbf{h}'), \quad (5)$$

where  $\phi_{FF}$  is a node-wise Feed-Forward MLP with output dimension  $d_h$  and  $\mathbf{h}'$  is an intermediate variable. Equation 5 can be seen as an independent block and be repeated multiple times with different parameters. We don't extend GAT to employ the multi-head attention mechanism (Vaswani et al. 2017) since we find that additional attention heads cannot help the final performance. We execute Equation 5 once and we set  $d_v = d_k$ . More implementation details are provided in Appendix A.

**Leaf Node Selection** Given the node features  $\mathbf{h}$ , we need to decide the leaf node indices for accommodating the current item  $n_t$ . Since the leaf nodes vary as the PCT keeps growing over time step  $t$ , we use a pointer mechanism (Vinyals et al. 2015) which is context-based attention over variable inputs to select a leaf node from  $\mathbf{L}_t$ . We still adopt Scaled Dot-Product Attention for calculating pointers, the global context feature  $\bar{h}$  is aggregated by a max operation on  $\mathbf{h}$ :  $\bar{h} = \frac{1}{N} \sum_{i=1}^N h_i$ . The global feature  $\bar{h}$

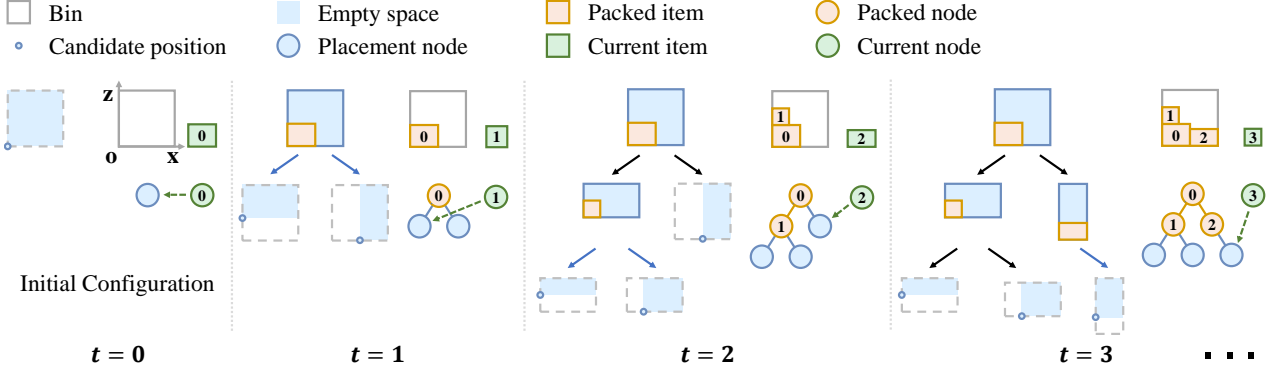


**Figure 1.** PCT expansion illustrated using a 2D example (in  $xoz$  plane) for simplicity, and the number of allowed orientations  $|\mathbf{O}|$  is 1 (see Appendix B for the 3D version). A newly added item introduces a series of empty spaces and new candidate placements are generated, e.g., the left-bottom corner of the empty space.

is projected to a query  $q$  by matrix  $W^q \in \mathbb{R}^{d_k \times d_h}$  and the leaf node features  $\mathbf{h}_L$  are utilized to calculate a set of keys  $k_L$  by  $W^k \in \mathbb{R}^{d_k \times d_h}$ . The compatibility  $\mathbf{u}_L$  of the query with all keys are:

$$q = W^q \bar{h}, \quad k_i = W^k h_i, \quad u_i = \frac{q^T k_i}{\sqrt{d_k}}. \quad (6)$$

Here  $h_i$  only comes from  $\mathbf{h}_L$ . The compatibility vector  $\mathbf{u}_L \in \mathbb{R}^{|\mathbf{L}_t|}$  represents the leaf node selection logits. The probability distribution over the PCT leaf nodes  $\mathbf{L}_t$  is:

$$\pi_\theta(\mathbf{L}_t | \mathcal{T}_t, n_t) = \text{softmax}(c_{clip} \cdot \tanh(\mathbf{u}_L)). \quad (7)$$

Following Bello et al. (2017), the compatibility logits are clipped with  $\tanh$ , where the range is controlled by hyperparameter  $c_{clip}$ , and finally normalized by softmax.

### 3.2 Markov Decision Process Formulation

The online 3D-BPP decision at time step  $t$  only depends on the current tuple  $(\mathcal{T}_t, n_t)$  and can be formulated as a Markov Decision Process (MDP), which is constructed with state  $\mathcal{S}$ , action  $\mathcal{A}$ , transition  $\mathcal{P}$ , and reward  $R$ . We solve this MDP with an end-to-end DRL agent. The MDP model is formulated as follows:

**State** The state  $s_t$  at time step  $t$  is represented as  $s_t = (\mathcal{T}_t, n_t)$ , where  $\mathcal{T}_t$  consists of the internal nodes  $\mathbf{B}_t$  and the leaf nodes  $\mathbf{L}_t$ . Each internal node  $b \in \mathbf{B}_t$  is a spatial configuration of size  $(s_b^x, s_b^y, s_b^z)$  and coordinate  $(p_b^x, p_b^y, p_b^z)$  corresponding to a packed item. The current item  $n_t$  is a size tuple  $(s_n^x, s_n^y, s_n^z)$ . Extra properties will be appended to  $b$  and  $n_t$  for specific packing preferences, such as density, item category, etc. The descriptor for leaf node  $l \in \mathbf{L}_t$  is a placement vector of size  $(s_o^x, s_o^y, s_o^z)$  and position coordinate  $(p^x, p^y, p^z)$ , where  $(s_o^x, s_o^y, s_o^z)$  indicates the sizes of  $n_t$  along each dimension after an axis-aligned orientation  $o \in \mathbf{O}$ . Only the packable leaf nodes that satisfy placement constraints are provided.

**Action** The action  $a_t \in \mathcal{A}$  is the index of the selected leaf node  $l$ , denoted as  $a_t = \text{index}(l)$ . The action space  $\mathcal{A}$  has the same size as  $\mathbf{L}_t$ . A surge of learning-based methods (Zhao et al. 2021) directly learn their policy on a grid world through discretizing the full coordinate space, where  $|\mathcal{A}|$  grows explosively with the accuracy of the discretization. Different from existing works, our action space solely depends on the leaf node expansion scheme and the packed items  $\mathbf{B}_t$ . Therefore, our method can be used to solve online 3D-BPP

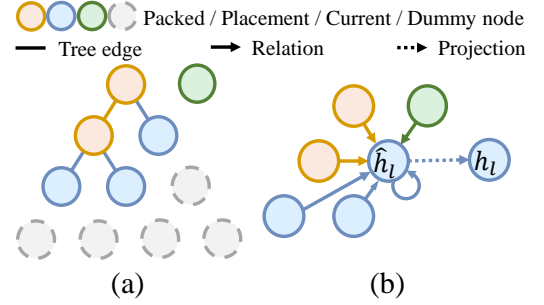


**Figure 2.** Batch calculation for PCT.

with continuous solution space. We also find that even if only an intercepted subset  $\mathbf{L}_{sub} \in \mathbf{L}_t$  is provided, our method can still maintain a good performance.

**Transition** The transition  $\mathcal{P}(s_{t+1}|s_t)$  is jointly determined by the current policy  $\pi$  and the probability distribution of sampling items. Our online sequences are generated on the fly from an item set  $\mathcal{I}$  in a uniform distribution. The transferability of our method on item sampling distributions different from the training one is discussed in Appendix C.

**Reward** Our reward function  $R$  is defined as  $r_t = c_r \cdot w_t$  once  $n_t$  is inserted into PCT as an internal node successfully; otherwise,  $r_t = 0$  and the packing episode ends. Here,  $c_r$  is a constant and  $w_t$  is the weight of  $n_t$ . The choice of  $w_t$  which depends on the customized needs. For simplicity and clarity, unless otherwise noted, we set  $w_t$  as the volume  $v_t$  of  $n_t$ , where  $v_t = s_n^x \cdot s_n^y \cdot s_n^z$ .

**Training Method** A DRL agent seeks a policy  $\pi(a_t|s_t)$  to maximize the accumulated discounted reward. Our DRL agent is trained with the ACKTR method (Wu et al. 2017). The actor weighs the leaf nodes  $\mathbf{L}_t$  and outputs the policy distribution  $\pi_\theta(\mathbf{L}_t | \mathcal{T}_t, n_t)$ . The critic maps the global context  $\bar{h}$  into a state value prediction to predict how much accumulated discount reward the agent can get from  $t$  and helps the training of the actor. The action  $a_t$  is sampled from the distribution  $\pi_\theta(\mathbf{L}_t | \mathcal{T}_t, n_t)$  for training, and we take the argmax of the policy for the test.

ACKTR runs multiple parallel processes for gathering on-policy training samples. The node number  $N$  of each sample varies with the time step  $t$  and the packing sequence of each process. For batch calculation, we fulfill PCT to a fixed length with dummy nodes, as illustrated by Figure 2 (a). These redundant nodes are eliminated by masked attention (Velickovic et al. 2018) during the feature

calculation of GAT. The aggregation of  $\mathbf{h}$  only happens on the eligible nodes. For preserving node spatial relations, state  $s_t$  is embedded by GAT as a fully connected graph as Figure 2 (b), without any inner mask operation. More implementation details are provided in Appendix A.

### 3.3 Recursive Packing for Large-Scale BPP

The enormous NP-hard solution space and the long sequence of decision-making make learning large-scale packing policies a formidable challenge. We propose *recursive packing*, which decomposes the large-scale  $\mathcal{T}$  into a set of smaller sub-trees  $\mathbf{T} = \{\mathcal{T}^1, \dots, \mathcal{T}^n\}$ . These sub-problems are solved in parallel using a pre-trained PCT model  $\pi_\theta$ , and the local solutions are then integrated to tackle the original  $\mathcal{T}$ . This approach alleviates the problem scale challenges while preserving the solution quality of  $\pi_\theta$ .

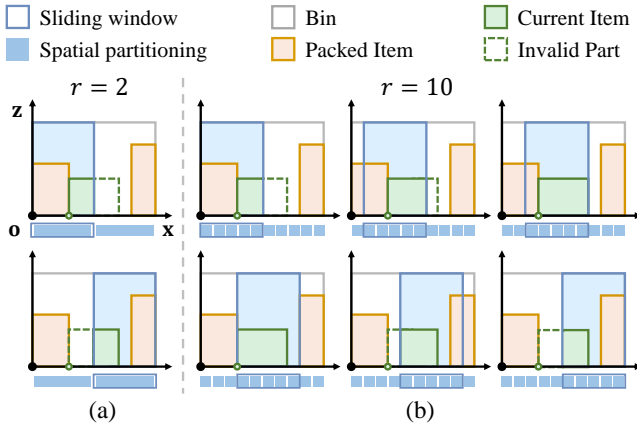


**Figure 3.** Problem decomposition based on sliding windows, illustrated in the  $xoz$  plane. Low-resolution decomposition (a) results in the loss of solutions, while fine-grained partitioning (b) clearly increases computational overhead.

For problem decomposition, an intuitive approach is to divide the bin  $C$  into uniform sections with resolution  $r$  along each dimension, and maintain a sliding window that traverses the entire bin space in a convolution-like manner, resulting in smaller sub-bins  $\mathbf{c} = \{c^1, \dots, c^n\}$ . Each  $c^i$ , along with its overlapped packed items  $\mathbf{B}^i$  and empty space  $\mathbf{L}^i$ , is treated as a sub-problem  $\mathcal{T}^i$ . While this decomposition is intuitive, it's not aware of the in-bin spatial distribution, leading to potential degradation in solution quality. Figure 3 (a) gives a demonstration for this, solutions that exist in the original bin  $C$  are no longer feasible in any of the decomposed sub-bin  $c^i$ . Although finer-grained partitioning can to some extent avoid this (Figure 3 (b)), it also leads to a  $O(r^6)$  space complexity, significantly increasing the number of sub-problems and computational costs. Even more, for problems requiring decisions in continuous domains, fine-grained partitioning is inherently infeasible.

However, for PCT, the decomposition of large-scale packing is natural and efficient. We adopt Empty Maximal Space (EMS), where each (previous) leaf node corresponds to a cube-shaped empty space that can be treated as a sub-bin. Given the current item  $n$  and a large-scale  $\mathcal{T}$ , the decomposition begins at a random leaf node  $l \in \mathcal{T}$  and backtracks upward. The backtrack stops at an internal node  $b^v$  whose sub-tree size  $|\mathcal{T}^v|$  exceeds a set threshold  $\tau$ . At this point, the historical EMS  $l^v$  accommodating  $b^v$  can

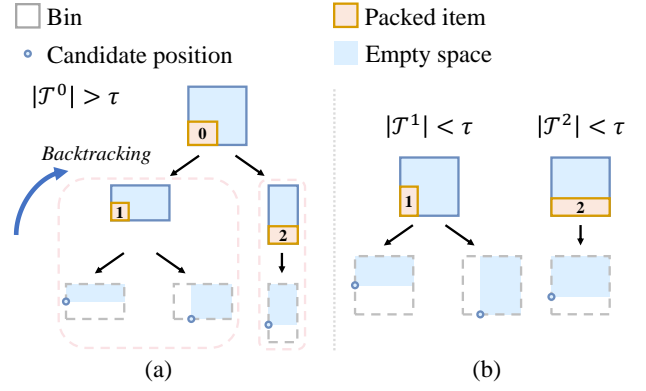


**Figure 4.** Recursive packing. The PCT  $\mathcal{T}^0$  with item 0 as the root exceeds the given threshold  $\tau = 2$ . (a) We backtrack from the leaf node upwards until the maximum size of sub-trees,  $\{\mathcal{T}^1, \mathcal{T}^2\}$ , is smaller than  $\tau$ . (b) Each sub-tree is normalized so that its dimensions can be mapped back to the original bin  $C$ .

be treated as a sub-bin  $c^v$ . After sub-bin determination, we detect whether any node of  $\mathcal{T}$  overlaps with  $c^v$ , and these overlaps are inherited as internal and leaf nodes of  $\mathcal{T}^v$  now viewed as a new sub-problem. This backtrack repeats iteratively until all leaf nodes  $\mathbf{L}$  are assigned to at least one sub-tree, ensuring that all possible solutions are retained and resulting in the sub-problem set  $\mathbf{T}$ . Figure 4 (a) provides an illustration of recursive packing with  $\tau = 2$ .

Since PCT supports decision-making in continuous domain, the configuration node of  $\mathcal{T}^v$  can be normalized back to the size of the original bin  $C$ , resulting in  $\hat{\mathcal{T}}^v$ . This enables the pre-trained policy  $\pi_\theta$  to well adapt to sub-problems and generate high-quality solutions. The nodes  $b^v, l^v, n^v \in \mathcal{T}^v$  can be normalized as:

$$\begin{aligned}\hat{b}^v &= (b^v - \text{FLB}(c^v)) \cdot S/s^v, \\ \hat{l}^v &= (l^v - \text{FLB}(c^v)) \cdot S/s^v, \\ \hat{n}^v &= n \cdot S/s^v,\end{aligned}\tag{8}$$

where  $S \in \mathbb{R}^3$  represents the size of the original bin  $C$  and  $s^v \in \mathbb{R}^3$  the size of sub-bin  $c^v$ . Function  $\text{FLB}(c^v)$  denotes the FLB coordinates of  $c^v$ . This normalization for  $\mathcal{T}^v$  is illustrated in Figure 4 (b).

**Spatial Ensemble** Given sub-problems  $\mathbf{T}$ , the solution for  $\mathcal{T}_i \in \mathbf{T}$  can be generated using a pre-trained policy  $\pi_\theta(\cdot | \hat{\mathcal{T}}_i, \hat{n})$ . These solutions need to be integrated to conduct a global placement. Zhao et al. (2021) propose evaluating placement quality in multi-bin decision scenarios utilizing the learned state value approximator  $V(c_t, n_t) = \mathbb{E}[\sum_{k=0}^{\infty} \gamma^k r_{t+k}]$ , which captures the cumulative space utilization achievable within bin  $c$  in the future after placing the current item  $n$  in  $c$ . Here  $\gamma \rightarrow 1$  is the reward discount factor. However, such a multi-bin decision approach assumes that bins are independent and do not affect each other, which obviously no longer holds in recursive packing. Moreover, the sub-bin only provides local placement evaluation, which does not necessarily represent the global optimality. As illustrated in Figure 5 (a), from the view of sub-bin  $c_1$ , the current item is compactly placed. However, from the global view of bin  $C$  (Figure 5 (b)), unused space exists beneath the current item which cannot be utilized for subsequent packing due to the top-down robot packing requirement, indicating a sub-optimal solution.



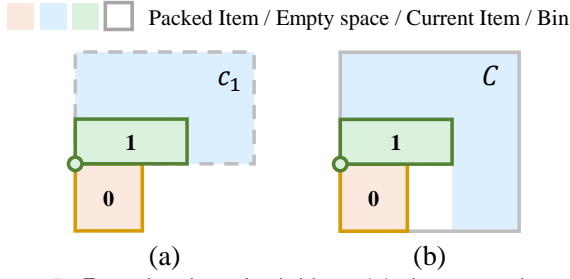


**Figure 5.** From the view of sub-bin  $c_1$  (a), the current item is optimally placed, but for the global view of bin  $C$  (b), unused space beneath the item exists which can no longer be utilized.

Based on the above observations, we propose *spatial ensemble*, which evaluates a placement via ensembling multiple sub-bins' views. We denote  $\Phi(l, c^i)$  as the score function for evaluating the value of leaf node  $l$  within sub-bin  $c^i$ ; the larger the better. This  $\Phi$  function can be defined with any customized criteria to represent industrial preferences. The optimal placement  $l^*$  is determined by selecting the leaf node with the best worst score across all sub-bins:

$$l^* = \arg \max_{l \in \mathbf{L}} \min_{c_i \in \mathbf{C}} \Phi(l, c_i). \quad (9)$$

It is important to note that  $\Phi(l, c_i)$  are not comparable across different sub-bins. For example, using the state value function  $V(\cdot)$ , the score for nearly full sub-bins approaches zero, while the score for an empty sub-bin may be close to volume  $|C|$ . This discrepancy in score ranges introduces comparison unfairness. To avoid this, we replace  $\Phi(l, c_i)$  from absolute values to ascending rank orders among all leaf nodes in a sub-bin  $c_i$ , denoted as  $\tilde{\Phi}(l, c_i) = \text{rank}_{\mathbf{L}_i}(\Phi(l, c_i))$ . The same leaf node  $l$  can appear in multiple sub-bins, and we select its worst rank as its final evaluation, with  $l^* = \arg \max_{l \in \mathbf{L}} \min_{c_i \in \mathbf{C}} \tilde{\Phi}(l, c_i)$ .

To maximize space utilization, we adopt the action probabilities output by the policy  $\pi(\cdot)$  as packing preferences  $\Phi$ . Since items within sub-bins no longer follow a fixed size distribution, we introduce a multi-scale training mechanism. During training, the policy is randomly exposed to item distributions of large, medium, and small sizes. After each packing episode, the size distribution changes, so the policy must adapt to these variations during training and enhance its adaptability to unseen sizes at test time.

### 3.4 Uniform Planning for BPP Variations

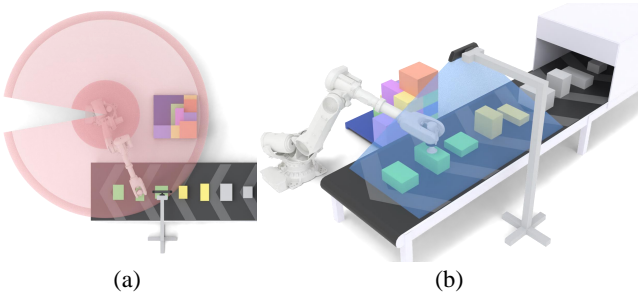


**Figure 6.** Item operation attributes for packing. The green items within the robotic arm's reach are selectable. Yellow items are previewed items and gray items are unknown.

Industrial packing takes various settings, and training a dedicated model for each is difficult to transfer to the others. A unified framework for solving different BPP variations

is highly desirable. Kagerer et al. (2023) provide a clear classification of mainstream packing problems based on item operation attributes. For robot packing, items are categorized as selectable, previewed, or unknown, determined by the camera field of view  $Fov_c$  and the robot's arm reach  $R_r$ , as illustrated in Figure 6. Selectable items are within the robot's reach  $R_r$ , as indicated by green items in the pink region of Figure 6 (a). Previewed items (yellow) are within the camera's view but outside the robot's reach, represented by the blue cone in Figure 6 (b). Unknown items lie outside  $Fov_c$  and are colored in gray. The total item number is  $|\mathcal{I}|$ , with the number of selectable, previewed, and unseen items represented by  $s = |\mathcal{R}_r|$ ,  $p = |Fov_c| - |\mathcal{R}_r|$ , and  $u = |\overline{Fov_c}|$ , respectively. A summary of the classification of mainstream packing problems is provided in Table 1.

**Table 1.** Mainstream packing problems. "Sel.", "Prev", and "Un." denote previewed, selectable, and unseen items.

Sel.	Prev.	Un.	Problem
$s = 1$	$p = 0$	$u > 0$	Online packing (Seiden 2002)
$s = 1$	$p > 0$	$u > 0$	Lookahead packing (Grove 1995)
$s > 1$	$p = 0$	$u > 0$	Buffering packing (Puche and Lee 2022)
$s =  \mathcal{I} $	$p = 0$	$u = 0$	Offline packing (Martello et al. 2000)

A genuine problem-solving process involves the repeated use of available information to initiate exploration, which discloses, in turn, more information until a way to attain the solution is finally discovered (Newell et al. 1959). We propose modeling various packing as model-based planning (MBP) (Mayne et al. 2000; Silver et al. 2016), where different item operation attributes are explicitly represented as distinct planning constraints. This allows different BPP variations to be solved within a unified framework and eliminates the need to introduce or adjust decision modules.

We first formalize offline 3D-BPP, where all items are selectable, as a planning problem. An intuitive approach is performing a traversal tree search over all packing orders and positions for all items  $\mathcal{I}$ . Each path of the search tree represents a possible solution, and we choose the one with the highest accumulated space utilization  $\sum_{i=0}^{|\mathcal{I}|} v_i$  for execution. This brute force search has a computational complexity of  $O(|\mathcal{I}|! \cdot |\mathcal{A}|^{|\mathcal{I}|})$ , where  $|\mathcal{A}|$  represents action space size. Leveraging the pre-trained policy model  $\pi_\theta$ , which determines item position, the search can be simplified to only consider item order, as exhibited in Figure 7 (a), lowering the complexity to  $O(|\mathcal{I}|!)$ . The constraints for planning selectable items are as follows:

1. Enumerate the placement order of items, with path node locations predicted by  $\pi_\theta$ .
2. Items are placed based on the node sequence of the planned path. The planning only conducts once.

Buffering packing can be considered a direct extension of offline packing, where unknown items should be additionally considered. These items cannot be explicitly included as tree nodes. We use the state value function  $V(\cdot)$  to implicitly estimate their distribution and future values. For  $s$  items within  $Fov_c$ , their placement order can still be enumerated during the planning, while items outside of  $Fov_c$  are all modeled as a single leaf node in the path end, as shown in Figure 7 (b). The value of each path is calculated by the sum

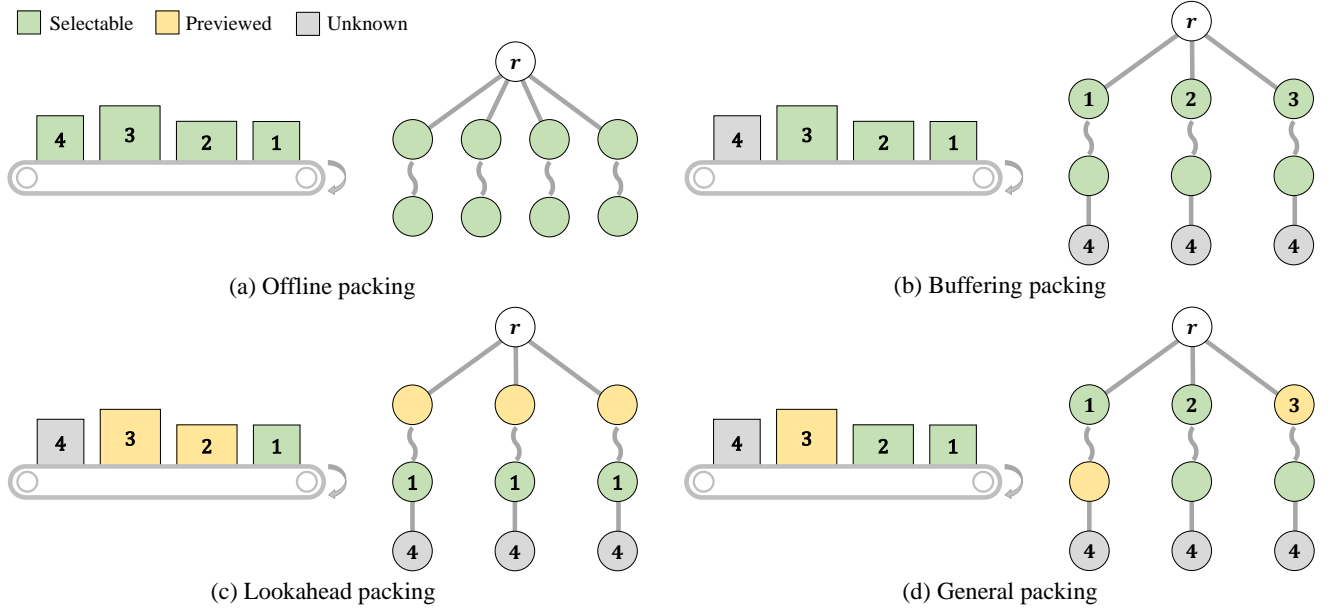


**Figure 7.** Mainstream BPP variations—offline (a), buffering (b), and lookahead (c)—can be modeled as search trees without conflicting planning constraints. We solve them out of the box via a unified framework (d) powered by a pre-trained PCT model.

of item volumes in the path and the value of the leaf node, i.e.,  $\sum_{i=0}^s v_i + V(\cdot)$ . Since future arrival exist, the planning follows the principle of MBP, where only the first node of the selected path is executed and the search reinitializes when a new item arrives. The additional planning constraints when introducing unknown items are summarized as:

1. All unknown items are modeled as leaf nodes of the search tree with their values estimated by  $V(\cdot)$ .
2. For each time step, only the first path node is executed, and planning restarts in the next.

Now we discuss lookahead packing when items in range  $Fov_c - R_r$  exist. These  $p$  items can be directly incorporated in the search tree for enumeration (Figure 7 (c)), accounting for future item arrival before packing the current one. The path with the highest score  $\sum_{i=0}^{s+p} v_i + V(\cdot)$  is selected. However, previewed items cannot be really placed, introducing additional search constraints:

1. Following top-down packing, the policy  $\pi_\theta$  must not place selectable items above previewed items.
2. For the selected path, only its first selectable node is executed, even if it starts with a previewed node.

We can find that these planning constraint for different operation attributes are compatible and can be integrated into a unified framework, which can be applied to general packing scenarios where  $p \geq 0$ ,  $s \geq 1$ , and  $u \geq 0$ , as illustrated in Figure 7 (d). We denote this unified search tree as **Tree of Packing (ToP)**. To ensure that the planning meets the real-time requirements of industrial packing, we introduce Monte Carlo Tree Search (MCTS) (Silver et al. 2016, 2017) which reduces the time complexity of the brute-force search from  $O(|p + s|!)$  to  $O((p + s) \cdot m)$ . Here  $m$  is the number of sampled paths. During planning, MCTS at adjacent time steps may share the same part of paths (i.e., item sequences). We maintain a global cache that stores previously visited paths to avoid redundant computations. This approach nearly halve the decision time costs.

## 4 Experiments

In this section, we first present PCT performance combined with different leaf node expansion schemes. We then highlight the advantages of the structured packing representation, including improved node spatial relation representations and a more flexible action space. Next, we validate the effectiveness of PCT-driven planners in solving industrial packing problems, specifically large-scale packing and different variations of BPP setting. Finally, we introduce our real-world packing robot in an industrial warehouse, carefully designed to meet constrained placement and transportation stability.

**Baselines** Although there are very few online packing implementations publicly available, we still do our best to collect or reproduce various online 3D-BPP algorithms, both heuristic and learning-based, from potentially relevant literature. We help the heuristics to make pre-judgments of placement constraints, e.g., stability, in case of premature downtime. The learning-based agents are trained until there are no significant performance gains. All methods are implemented in Python and tested on 2000 instances with a desktop computer equipped with a Gold 5117 CPU and a GeForce TITAN V GPU.

**Datasets** Some baselines (Karabulut and Inceoglu 2004; Wang and Hauser 2019b) need to traverse the entire coordinate space to find the optimal solution, and the running costs explode as the spatial discretization accuracy increases. To ensure that all algorithms are runnable within a reasonable period, we use the discrete dataset proposed by Zhao et al. (2021) without special declaration. The bin sizes  $S^d$  are set to 10 with  $d \in \{x, y, z\}$  and the item sizes  $s^d \in \mathbb{Z}^+$  are not greater than  $S^d/2$  to avoid over-simplification. Our performance on the continuous dataset will be reported in Section 4.3. Considering that there are many practical scenarios of 3D-BPP, we choose three representative ones:

**Setting 1:** Following Zhao et al. (2022b), stability of  $\mathbf{B}_t$  is verified when  $n_t$  is placed. For robot manipulation convenience, only two horizontal orientations ( $|\mathbf{O}| = 2$ ) are allowed for top-down placement.



*Setting 2:* Following [Martello et al. \(2000\)](#), item  $n_t$  only needs to satisfy Constraints 2 and 3. Arbitrary orientation ( $|\mathbf{O}| = 6$ ) is allowed here. This is the most common setting in the 3D-BPP literature.

*Setting 3:* Building on *setting 1*, each item  $n_t$  is assigned an additional density property  $\rho$  uniformly sampled from  $(0, 1]$ . This density information is incorporated into the descriptors of both  $\mathbf{B}_t$  and  $n_t$ .

#### 4.1 Performance of PCT Policies

We first report the performance of PCT combined with different leaf node expansion schemes. Three existing schemes which have proven to be both efficient and effective are adopted here: Corner Point (CP), Extreme Point (EP), and Empty Maximal Space (EMS). These schemes are all related to boundary points of packed items  $b \in \mathbf{B}_t$  along the  $d$  axis. We combine these boundary points to get the superset, namely *Event Point* (EV). See Appendix B for details and learning curves. We incorporate these schemes into our PCT model. Although the number of generated leaf nodes is reasonable, we only randomly intercept a subset  $\mathbf{L}_{sub_t} \subset \mathbf{L}_t$  if  $|\mathbf{L}_t|$  exceeds a certain length, for saving computing resources. This interception length is constant during training and determined by a grid search (GS) during the test. See Appendix A for details. The performance comparisons are summarized in Table 2.

Although PCT grows under the guidance of heuristics, the combinations of PCT with EMS and EV still learn effective policies outperforming all baselines by a large margin across all settings. Note that the closer the space utilization is to 1, the more difficult online 3D-BPP is. It is interesting to see that policies guided by EMS and EV even exceed the performance of the full coordinate space (FC), which is expected to be optimal. This demonstrates that a good leaf node expansion scheme reduces the complexity of packing and helps DRL agents achieve better performance. To prove that the interception of  $\mathbf{L}_t$  will not harm the final performance, we train agents with full leaf nodes derived from the EV scheme (EVF), and the test performance is slightly worse than the intercepted cases. We conjecture that the interception keeps the final performance may be caused by two reasons. First, sub-optimal solutions for online 3D-BPP exist even in the intercepted set  $\mathbf{L}_{sub}$ . In addition, the randomly chosen leaf nodes force the agent to make new explorations in case the policy  $\pi$  falls into the local optimum.

The performance of [Zhao et al. \(2022b\)](#) deteriorates quickly in *setting 2* and *setting 3* due to the multiplying orientation space and insufficient state representation separately. Running costs, scalability performance, behavior understanding, and visualized results can be found in Appendix C. We also repeat the same experiment as [Zhang et al. \(2021\)](#), which packs items sampled from a pre-defined item set  $|\mathcal{I}| = 64$  in *setting 2*. While the method of [Zhang et al. \(2021\)](#) packs on average 15.6 items and achieves 67.0% space utilization, our method packs 19.7 items with a space utilization of 83.0%. Although EV sometimes yields better performance, we provide a detailed explanation in Appendix B that its computational complexity is quadratic, whereas EMS’s complexity is linear to internal nodes  $|\mathbf{B}|$ . Therefore, we choose EMS as the default scheme.

#### 4.2 Benefits of Tree Presentation

Here we verify that the PCT representation does help online 3D-BPP tasks. For this, we embed each space configuration node independently like PointNet ([Qi et al. 2017](#)) to prove that the node spatial relations help the final performance. We also deconstruct the tree structure into node sequences and embed them with Ptr-Net ([Vinyals et al. 2015](#)), which selects a member from serialized inputs, to indicate that the graph embedding fashion fits our tasks well. We have verified that an appropriate choice of  $\mathbf{L}_t$  makes DRL agents easy to train, then we remove the internal nodes  $\mathbf{B}_t$  from  $\mathcal{T}_t$ , along with its spatial relations with other nodes, to prove  $\mathbf{B}_t$  is also a necessary part. We choose EV as the leaf node expansion scheme here. The comparisons are summarized in Table 3.

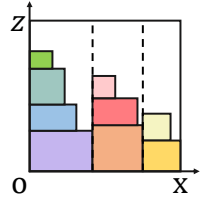
If we ignore the spatial relations between the PCT nodes or only treat the state input as a flattened sequence, the performance of the learned policies will be severely degraded. The presence of  $\mathbf{B}$  functions more on *setting 1* and *setting 3* since *setting 2* allows items to be packed in any empty spaces without considering constraints with internal nodes. This also confirms that a complete PCT representation is essential for online 3D-BPP of practical needs.

#### 4.3 Performance on Continuous Dataset

The most concerning issue about online 3D-BPP is its solution space limit. Given that most learning-based methods can only work in a limited, discrete space, we directly test our method in a continuous bin with sizes  $S^d = 1$  to demonstrate our superiority. Due to the lack of public datasets for online 3D-BPP issues, we generate item sizes through a uniform distribution  $s^d \sim U(a, S^d/2)$ , where  $a$  is set to 0.1 in case endless items are generated.

Specifically, for 3D-BPP instances where stability is considered, the diversity of item size  $s^z$  needs to be controlled. If all subsets of  $\mathbf{B}_t$  meet:

$$\sum_{i \in \mathbf{B}_{sub1}} s_i^z \neq \sum_{i \in \mathbf{B}_{sub2}} s_i^z, \quad (10)$$



where  $\mathbf{B}_{sub1} \neq \mathbf{B}_{sub2}$ ,  $\mathbf{B}_{sub1}, \mathbf{B}_{sub2} \in \mathbf{B}_t$ . This means the partition problem ([Korf 1998](#)) has no solutions, and any packed items cannot form a new plane for providing support in the direction of gravity and the available packing areas shrink. Excessive diversity of  $s^z$  will degenerate 3D-BPP into 1D-BPP as presented in the above toy demo. To prevent this degradation from leading to the underutilization of the bins, we sample  $s^z$  from a finite set  $\{0.1, 0.2, \dots, 0.5\}$  on *setting 1* and *setting 3* in this section.

We find that some heuristic methods like OnlineBPH ([Ha et al. 2017](#)) also have the potential to work in the continuous domain. We improve these methods as our baselines. Another intuitive approach for online packing with continuous domain is driving a DRL agent to sample actions from a Gaussian distribution (GD) and output continuous coordinates directly. The test results are summarized in Table 4. Although the infinite continuous-size item set ( $|\mathcal{I}| = \infty$ ) increases the difficulty of the problem and reduces the performance of all methods, our method still performs the best among all competitors. The DRL agent which directly outputs continuous actions cannot even converge, and their

**Table 2.** Performance comparisons. “Uti.” and “Num.” represent the average space utilization and the average number of packed items, respectively. “Var.” ( $\times 10^{-3}$ ) refers to the variance of “Uti.” and “Gap” indicates the difference relative to the best “Uti.” across all methods. “Random” refers to placements selected randomly from all possible coordinates. DBL, LSAH, MACS, BR, and HM are heuristic methods proposed by Karabulut and Inceoglu (2004), Hu et al. (2017), Hu et al. (2020), Zhao et al. (2021), and Wang and Hauser (2019b). CDRL presents the constrained deep reinforcement learning method proposed by Zhao et al. (2022b).

Method	Setting 1				Setting 2				Setting 3				
	Uti. ↑	Var. ↓	Num. ↑	Gap ↓	Uti. ↑	Var. ↓	Num. ↑	Gap ↓	Uti. ↑	Var. ↓	Num. ↑	Gap ↓	
Heuristic	Random	36.7%	10.3	14.9	51.7%	38.6%	8.3	15.7	55.1%	36.8%	10.6	14.9	51.4%
	BR	49.0%	10.8	19.6	35.5%	56.7%	6.6	22.6	34.1%	48.9%	10.7	19.5	35.4%
	OnlineBPH	52.1%	20.1	20.6	31.4%	59.9%	10.4	23.8	30.3%	51.9%	20.2	20.6	31.4%
	LSAH	52.5%	12.2	20.8	30.9%	65.0%	6.1	25.6	24.4%	52.4%	12.2	20.7	30.8%
	HM	57.6%	11.5	24.1	24.2%	66.1%	8.4	25.9	23.1%	56.5%	11.2	22.3	25.4%
	MACS	57.7%	10.5	22.6	24.1%	50.8%	8.8	20.1	40.9%	57.7%	10.6	22.6	23.8%
	DBL	60.5%	8.8	23.8	20.4%	70.6%	7.9	27.8	17.9%	60.5%	8.9	23.8	20.1%
Learning-based	CDRL	70.9%	6.2	27.5	6.7%	70.3%	4.3	27.4	18.3%	59.6%	5.4	23.1	21.3%
	PCT & CP	69.4%	5.4	26.7	8.7%	81.8%	2.0	31.3	4.9%	69.5%	5.4	26.7	8.2%
	PCT & EP	71.9%	6.6	27.8	5.4%	78.1%	3.8	30.3	9.2%	72.2%	5.8	27.9	4.6%
	PCT & FC	72.4%	4.7	28.0	4.7%	76.9%	3.3	29.7	10.6%	69.8%	5.3	27.1	7.8%
	PCT & EV	<b>76.0%</b>	<b>4.2</b>	<b>29.4</b>	<b>0.0%</b>	85.3%	2.1	32.8	0.8%	<b>75.7%</b>	<b>4.6</b>	<b>29.2</b>	<b>0.0%</b>
	PCT & EMS	75.8%	4.4	29.3	0.3%	<b>86.0%</b>	<b>1.9</b>	<b>33.0</b>	<b>0.0%</b>	75.5%	4.7	29.2	0.3%

**Table 3.** The graph embedding of complete PCT helps the final performance.

Presentation	Setting 1				Setting 2				Setting 3			
	Uti. $\uparrow$	Var. $\downarrow$	Num. $\uparrow$	Gap $\downarrow$	Uti. $\uparrow$	Var. $\downarrow$	Num. $\uparrow$	Gap $\downarrow$	Uti. $\uparrow$	Var. $\downarrow$	Num. $\uparrow$	Gap $\downarrow$
PointNet	69.2%	6.7	26.9	8.9%	78.9%	3.2	30.5	7.5%	71.5%	5.3	27.7	5.5%
Ptr-Net	64.1%	10.0	25.1	15.7%	77.5%	4.1	30.1	9.1%	63.5%	7.9	24.8	16.1%
PCT ( $\mathcal{T}/\mathbf{B}$ )	70.9%	5.9	27.5	6.7%	84.1%	2.6	32.3	1.4%	70.6%	5.3	27.4	6.7%
PCT ( $\mathcal{T}$ )	<b>76.0%</b>	<b>4.2</b>	<b>29.4</b>	<b>0.0%</b>	<b>85.3%</b>	<b>2.1</b>	<b>32.8</b>	<b>0.0%</b>	<b>75.7%</b>	<b>4.6</b>	<b>29.2</b>	<b>0.0%</b>

**Table 4.** Online 3D-BPP with continuous solution space.

Method		Setting 1				Setting 2				Setting 3			
		Uti. $\uparrow$	Var. $\downarrow$	Num. $\uparrow$	Gap $\downarrow$	Uti. $\uparrow$	Var. $\downarrow$	Num. $\uparrow$	Gap $\downarrow$	Uti. $\uparrow$	Var. $\downarrow$	Num. $\uparrow$	Gap $\downarrow$
Heu.	BR	40.9%	7.4	16.1	37.5%	45.3%	5.2	17.8	31.7%	40.9%	7.3	16.1	38.6%
	OnlineBPH	43.9%	14.2	17.2	32.9%	46.1%	6.8	18.1	30.5%	43.9%	14.2	17.2	34.1%
	LSAH	48.3%	12.1	18.7	26.1%	58.7%	4.6	22.8	11.5%	48.4%	12.2	18.8	27.3%
DRL	GD	5.6%	–	2.2	91.4%	7.5%	–	2.9	88.7%	5.2%	–	2.1	92.2%
	PCT & EV	<b>65.4%</b>	<b>3.3</b>	<b>25.0</b>	<b>0.0%</b>	65.0%	2.6	26.4	2.0%	65.8%	3.6	25.1	2.7%
	PCT & EMS	65.3%	4.4	24.9	0.2%	<b>66.3%</b>	<b>2.3</b>	<b>27.0</b>	<b>0.0%</b>	<b>66.6%</b>	<b>3.3</b>	<b>25.3</b>	<b>0.0%</b>

variance is not considered. Our work is the first learning-based method that solves online 3D-BPP with continuous solution space successfully.

#### 4.4 More Complex Practical Constraints

To further demonstrate that PCT effectively handles complex constraints, we conduct experiments extending PCT to online 3D-BPP with practical constraints, including isle friendliness, load balancing, and load bearing constraints proposed by Gzara et al. (2020), kinematic constraints (Martello et al. 2007), bridging constraints (Shin et al. 2016), and height uniformity:

- *Isle Friendliness* stipulates that items of the same category should be packed closely as possible. The item weight is defined as  $w_t = \max(0, v_t - c \cdot \text{dist}(n_t, \mathbf{B}_t))$ . Here  $c$  is a constant and the objective function  $\text{dist}(n_t, \mathbf{B}_t)$  means the average distance between  $n_t$  and the items of the same category in  $\mathbf{B}_t$ . Category information is appended to the descriptors of  $\mathbf{B}_t$  and  $n_t$ . Four item categories are tested here.

- *Load Balancing* dictates that the packed items should have an even mass distribution within the bin. The item weight is set as  $w_t = \max(0, v_t - c \cdot \text{var}(n_t, \mathbf{B}_t))$ . Object

$\text{var}(n_t, \mathbf{B}_t)$  is the variance of the mass distribution of the packed items on the bottom of the bin.

- *Load-bearing Constraint* considers that items placed above do not exert excessive weight on those below. The force on each item is simulated using physics engine (Coumans and Bai 2016), and the item weight is  $w_t = \max(0, v_t - c \cdot f(n_t, \mathbf{B}_t))$ , where  $f(n_t, \mathbf{B}_t)$  represents the force born by  $n_t$ .

- *Kinematic Constraint* minimizes the impact of placed items on the robot’s subsequent motions. Instead of time-consuming motion planning (Görner et al. 2019), we use the safe position reward  $V_{\text{safe}}$  proposed by Zhao et al. (2022b). The item weight is  $w_t = v_t + c \cdot V_{\text{safe}}$ .

- *Bridging Constraint* requires items to be stacked interlockingly, improving stability by distributing the center of gravity, increasing the contact area, and enhancing friction (Page 1981). The number of items  $b \in \mathbf{B}_t$  that contribute to bridging  $n_t$  is summed up as  $\text{bridge}(n_t, \mathbf{B}_t)$ , and the item weight is  $w_t = v_t + c \cdot \text{bridge}(n_t, \mathbf{B}_t)$ .

- *Height Uniformity* ensures even height distribution of items in the bin. The item weight is  $w_t = \max(0, v_t - c \cdot$

**Table 5.** Online 3D-BPP with practical constraints. “Obj.” means the task-specific objective score, which is the primary focus of this comparison. Whether a higher or lower value is preferable depends on the task, with the preference indicated by arrows next to the task name. For load balancing and height uniformity tasks, the objective score is scaled by  $\times 10^3$  and  $\times 10^2$ , respectively. “Imp.” indicates the percentage improvement in “Obj.” compared to a random placement policy.

Constraints	Method	Setting 1				Setting 2				Setting 3			
		Obj.	Imp. ↑	Uti. ↑	Num. ↑	Obj.	Imp. ↑	Uti. ↑	Num. ↑	Obj.	Imp. ↑	Uti. ↑	Num. ↑
Isle Friendliness ↓	CDRL	0.20	31.0%	58.3%	22.5	0.19	20.8%	64.2%	24.8	0.20	48.7%	59.0%	22.8
	PCT	<b>0.15</b>	<b>48.3%</b>	<b>72.1%</b>	<b>29.0</b>	<b>0.08</b>	<b>66.6%</b>	<b>85.2%</b>	<b>32.8</b>	<b>0.15</b>	<b>61.5%</b>	<b>74.6%</b>	<b>28.8</b>
Load Balancing ↓	CDRL	3.32	41.7%	55.8%	21.6	3.11	32.1%	58.3%	22.5	1.42	21.5%	55.9%	21.7
	PCT	<b>1.40</b>	<b>75.4%</b>	<b>71.2%</b>	<b>27.7</b>	<b>0.69</b>	<b>84.9%</b>	<b>83.5%</b>	<b>32.3</b>	<b>0.22</b>	<b>87.8%</b>	<b>71.2%</b>	<b>27.7</b>
Height Uniformity ↓	CDRL	6.99	26.6%	53.3%	20.9	7.22	38.4%	54.4%	21.1	7.34	21.5%	54.4%	21.2
	PCT	<b>3.79</b>	<b>60.2%</b>	<b>74.3%</b>	<b>28.8</b>	<b>2.01</b>	<b>82.8%</b>	<b>83.5%</b>	<b>32.3</b>	<b>3.81</b>	<b>59.3%</b>	<b>73.1%</b>	<b>28.4</b>
Kinematic Constraints ↑	CDRL	0.77	35.1%	54.6%	21.2	0.53	−31.2%	60.0%	23.1	0.79	17.9%	56.5%	22.0
	PCT	<b>0.94</b>	<b>64.9%</b>	<b>72.8%</b>	<b>28.2</b>	<b>0.96</b>	<b>24.7%</b>	<b>84.8%</b>	<b>32.6</b>	<b>0.93</b>	<b>38.8%</b>	<b>74.6%</b>	<b>28.8</b>
Load Bearing Constraints ↓	CDRL	1.95	61.8%	51.8%	20.7	2.44	32.4%	50.3%	19.6	1.30	60.0%	44.7%	17.0
	PCT	<b>1.43</b>	<b>72.0%</b>	<b>69.8%</b>	<b>27.9</b>	<b>1.41</b>	<b>60.9%</b>	<b>80.6%</b>	<b>31.8</b>	<b>0.80</b>	<b>75.4%</b>	<b>68.7%</b>	<b>27.3</b>
Bridging Constraints ↑	CDRL	1.09	2.8%	59.3%	23.0	1.03	1.0%	60.8%	23.4	1.07	1.9%	59.7%	23.1
	PCT	<b>1.18</b>	<b>11.3%</b>	<b>69.2%</b>	<b>26.9</b>	<b>1.30</b>	<b>27.5%</b>	<b>80.6%</b>	<b>31.3</b>	<b>1.19</b>	<b>13.3%</b>	<b>69.0%</b>	<b>26.9</b>

$H_{\text{var}}$ ), where  $H_{\text{var}}$  is the variance of the heightmap inside the bin after packing the items  $n_t$ .

We adopt the learning-based method CDRL in Section 4.1 as the baseline, as heuristic methods primarily aim to maximize space utilization and are not flexible enough to handle additional constraints. The results are summarized in Table 5. PCT demonstrates strong adaptability to multiple complex constraints, achieving consistently higher objective scores. Its improvement over random placement (Imp.) clearly outperforms the baseline method, demonstrating that PCT effectively captures complex task constraints and is suitable for solving online packing in practical applications.

#### 4.5 Recursive Packing for Large Problems

We validate the effectiveness of recursive packing for large problem scales. To keep the validation focusing on problem decomposition and solution integration, we follow the standard packing setup (Martello et al. 2000) of setting 2. The method is tested on continuous domains with bin dimensions set to  $S^d = 1$ . The packing scale  $\bar{N}$  is maintained by sampling the item size from a uniform distribution  $\mathcal{U}(0, (8/\bar{N})^{\frac{1}{3}})$ . Sub-problems are decomposed recursively with a threshold  $\tau = 30$  and our spatial ensemble method integrates local solutions produced by pre-trained PCT models  $\pi_\theta$ . The experiments are conducted on  $\bar{N} \in \{200, 500, 1000\}$ . To date,  $\bar{N} = 500$  is the largest scale for learning-based online packing. For each  $\bar{N}$ , 100 test sequences are randomly generated, and all methods are tested on the same data. The test results are summarized in Table 6. We compare with baselines which can operate in the continuous domain, including BR (Zhao et al. 2021), OnlineBPP (Ha et al. 2017), and LSAH (Hu et al. 2017). Additionally, we evaluate the performance of the PCT model trained on the corresponding scale  $\bar{N}$ , labeled as PCT\*, and the performance of transferring a pre-trained PCT model  $\pi_\theta$  to large problem scales, labeled as PCT<sup>†</sup>.

As illustrated in Table 6, recursive packing excels on large problem scales, achieving consistently the best performance. Notably, as the problem scale  $\bar{N}$  increases, its performance continues to improve. Among all tested methods, only recursive packing and LSAH exhibit such improvements as the problem scale grows, with recursive

packing significantly outperforming LSAH. We visualize the large-scale packing results of recursive packing in Appendix D. For the smaller scale  $\bar{N} = 200$ , both PCT\* and PCT<sup>†</sup> behave satisfactorily. However, as  $\bar{N}$  increases, PCT\* quickly deteriorates, confirming training instability brought by long-sequence decision making and underscoring the necessity of problem decomposition. PCT<sup>†</sup> performs consistently across different problem scales, verifying its generalization ability.

To validate the necessity of spatial ensemble, we compare it with other solution integration schemes. These alternatives lack the inter-bin comparison. Instead, they directly select the sub-bin  $c$  with locally the highest score  $\Phi$ :

$$c = \arg \max_{c_i \in C} \Phi(c_i). \quad (11)$$

The pre-trained policy  $\pi$  then determines the placement in the selected sub-bin  $c$ . We test the following functions  $\Phi$ :

- **Maximum State Value:** The sub-bin  $c$  with the highest state value  $V(\cdot)$  is selected to place the current item  $n$ . A higher state value indicates higher future capacity. The score function is  $\Phi(c_i) = V(\hat{\mathcal{T}}_i)$ , where  $\hat{\mathcal{T}}_i$  is the normalized PCT representation within  $c_i$ .

- **Maximum Volume:** Similar to the minimum cost priority principle (Dijkstra 2022), the sub-bin  $c$  with the largest volume is selected. A larger volume indicates better filling of a sub-bin. From a divide-and-conquer perspective, effectively completing sub-tasks improves overall task performance. The score function is  $\Phi(c_i) = \sum_{\hat{b}_j \in \hat{\mathbf{B}}_i} \hat{s}_j^x \cdot \hat{s}_j^y \cdot \hat{s}_j^z$ , where  $\hat{s} \in \mathbb{R}^3$  is the normalized size of node  $\hat{b} \in \hat{\mathbf{B}}_i$ .

- **Maximum Return:** Inspired by the A\* algorithm (Hart et al. 1968) which considers both cost and future profits, we sum up the state value and volume of a sub-bin  $c$ . The score function is  $\Phi(c_i) = V(\hat{\mathcal{T}}_i) + \sum_{\hat{b}_j \in \hat{\mathbf{B}}_i} \hat{s}_j^x \cdot \hat{s}_j^y \cdot \hat{s}_j^z$ , reflecting the total reward of placing  $n$  in  $c$ .

- **Minimum Surface Area:** Unlike previous local evaluations, a global score function is introduced to minimize the surface area of packed items. A smaller surface area indicates a more compact stack. The function is:  $\Phi(c_i) = -(\tilde{S}_i^x \cdot \tilde{S}_i^y + \tilde{S}_i^x \cdot \tilde{S}_i^z + \tilde{S}_i^y \cdot \tilde{S}_i^z)$ , where  $\tilde{S}_i^d$  represents the maximum stack dimensions along axis  $d$  after placing item  $n$  in sub-bin  $c_i$ .

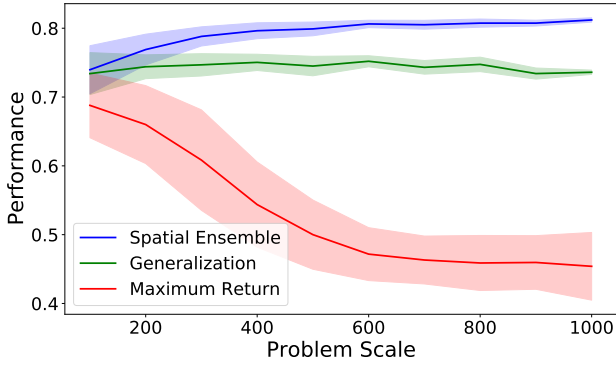
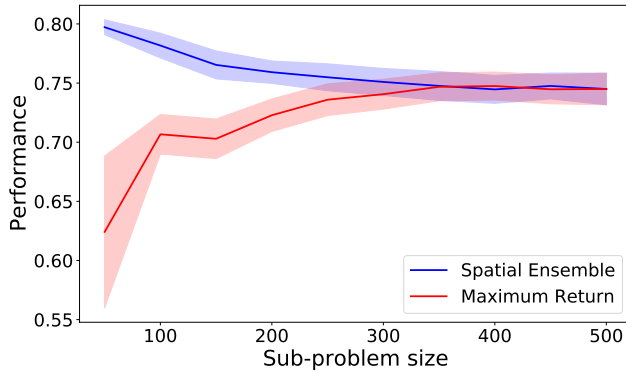
The results are summarized in Table 7. Locally evaluating sub-bins without inter-bin comparison leads to sub-optimal

**Table 6.** Performance comparisons on large packing scales.

Method	$\bar{N} = 200$				$\bar{N} = 500$				$\bar{N} = 1000$			
	Uti. $\uparrow$	Var. $\downarrow$	Num. $\uparrow$	Gap $\downarrow$	Uti. $\uparrow$	Var. $\downarrow$	Num. $\uparrow$	Gap $\downarrow$	Uti. $\uparrow$	Var. $\downarrow$	Num. $\uparrow$	Gap $\downarrow$
BR	50.6%	1.3	101.7	34.2%	49.6%	0.4	248.0	37.9%	49.3%	0.2	482.9	39.3%
OnlineBPH	40.1%	1.5	81.6	47.9%	38.6%	0.6	190.0	51.7%	40.1%	0.3	398.7	50.6%
LSAH	64.1%	1.4	128.4	16.6%	68.3%	0.5	341.6	14.5%	69.8%	0.1	681.7	14.0%
PCT*	72.3%	0.8	144.4	6.0%	74.4%	0.5	370.9	6.9%	56.4%	0.4	553.4	30.5%
PCT <sup>†</sup>	74.4%	<b>0.3</b>	147.8	3.3%	74.5%	0.2	371.1	6.8%	73.6%	0.1	719.1	9.4%
Recursive Packing	<b>76.9%</b>	0.5	<b>153.1</b>	<b>0.0%</b>	<b>79.9%</b>	<b>0.1</b>	<b>397.6</b>	<b>0.0%</b>	<b>81.2%</b>	<b>0.01</b>	<b>792.5</b>	<b>0.0%</b>

**Table 7.** Performance of different solution integration functions for ToP.

Integration Method	$\bar{N} = 200$				$\bar{N} = 500$				$\bar{N} = 1000$			
	Uti. $\uparrow$	Var. $\downarrow$	Num. $\uparrow$	Gap $\downarrow$	Uti. $\uparrow$	Var. $\downarrow$	Num. $\uparrow$	Gap $\downarrow$	Uti. $\uparrow$	Var. $\downarrow$	Num. $\uparrow$	Gap $\downarrow$
Maximum State Value	60.5%	1.5	121.2	21.3%	46.9%	1.3	234.5	41.3%	41.4%	1.2	411.3	49.0%
Maximum Return	66.2%	3.2	132.4	13.9%	50.0%	2.5	249.5	37.4%	45.4%	2.4	446.6	44.1%
Maximum Volume	66.6%	1.4	133.2	13.4%	61.5%	4.7	307.6	23.0%	48.7%	8.1	479.3	40.0%
Minimum Surface Area	65.4%	2.3	130.8	15.0%	55.5%	2.1	277.6	30.5%	49.7%	4.1	489.0	38.8%
Spatial Ensemble	<b>76.9%</b>	<b>0.5</b>	<b>153.1</b>	<b>0.0%</b>	<b>79.9%</b>	<b>0.1</b>	<b>397.6</b>	<b>0.0%</b>	<b>81.2%</b>	<b>0.01</b>	<b>792.5</b>	<b>0.0%</b>

**Figure 8.** Packing performance across different problem scales, with shaded regions around each curve representing performance variance; the wider the larger.**Figure 9.** Packing performance for varying sub-problem scale thresholds  $\tau$ , tested on problem scale  $\bar{N} = 500$ . As  $\tau$  nears  $\bar{N}$ , both algorithms degrade to direct transfer. Spatial ensemble benefits from problem decomposition, with smaller  $\tau$  improving performance, while maximum return shows the opposite.

performance. The minimum surface area alternative, while it evaluates globally, does not directly correlate with the objective of maximizing space utilization. These results emphasize the importance of effectively integrating local solutions. In contrast, our spatial ensemble method leverages inter-bin comparison to obtain global solution, resulting in significant performance advantage across different  $\bar{N}$ .

We also make comparisons with PCT<sup>†</sup>. Its performance consistently behaves worse than recursive packing. We provide performance curves in Figure 8, with wider shaded areas indicating higher variance. While recursive packing consistently improves with increasing problem scale, PCT<sup>†</sup> maintains performance similar to the training scale across all problem scales. We also visualize the performance of the integration method of maximum return, which performs worse as the problem scale grows and exhibits significant variance all the time.

We explore the impact of the sub-problem decomposition threshold  $\tau$  on final performance, with experiments conducted on  $\bar{N} = 500$ . As observed in Figure 9, increasing  $\tau$ , which makes sub-problem scale approach the original problem, causes both recursive packing and maximum return to degrade to the direct generalization performance of the pre-trained policy. The performance of recursive packing improves with finer decomposition, while the maximum return integration declines. This highlights the importance of solution integration choice.

#### 4.6 ToP Results on BPP Variations

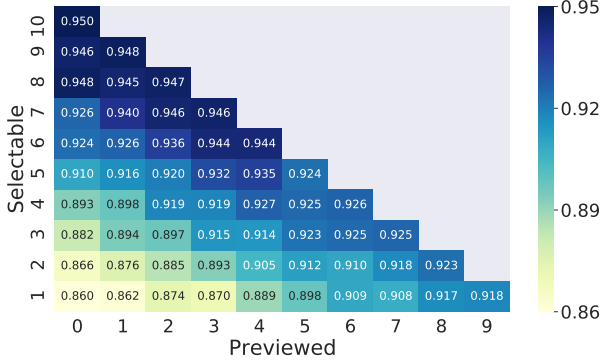
We evaluate the effectiveness of our unified planning framework, ToP, across different BPP variations. We compare ToP with state-of-the-art algorithms for each setting to validate its consistent superiority. We first conduct comparisons on packing forms with online properties with  $u > 0$ . For lookahead packing with  $s = 1, p > 0$ , we compare ToP with CDRL (Zhao et al. 2022b). For buffering packing with  $s > 1, p = 0$ , we compare it with TAP-NET++ (Xu et al. 2023). For general packing, where  $s \geq 1, p \geq 0$ , we adopt the O3DBP method proposed by Kagerer et al. (2023). Since most baselines operate in discrete domains, this experiment is conducted on the discrete dataset. Performance comparisons on the continuous-domain ICRA stacking challenge datasets are provided in Appendix C.

The comparison results across different packing settings are summarized in Table 8. ToP consistently delivers the best space utilization. We visualize ToP performance with varying selectable item number  $s$  and previewed item number  $p$  in Figure 10, based on experiments conducted



**Table 8.** Performance comparison across different BPP variations with online properties.

Method	Sel.	Prev.	Un.	Setting 1				Setting 2				Setting 3			
				Uti. $\uparrow$	Var. $\downarrow$	Num. $\uparrow$	Gap $\downarrow$	Uti. $\uparrow$	Var. $\downarrow$	Num. $\uparrow$	Gap $\downarrow$	Uti. $\uparrow$	Var. $\downarrow$	Num. $\uparrow$	Gap $\downarrow$
CDRL	1	9	> 0	82.5%	6.0	32.3	0.7%	75.0%	1.3	29.0	17.4%	68.4%	5.3	27.3	19.2%
ToP	1	9	> 0	<b>83.1%</b>	<b>5.6</b>	<b>32.5</b>	<b>0.0%</b>	<b>90.8%</b>	<b>1.1</b>	<b>35.3</b>	<b>0.0%</b>	<b>84.7%</b>	<b>1.9</b>	<b>33.1</b>	<b>0.0%</b>
O3DBP	5	5	> 0	53.1%	7.5	26.4	39.0%	60.4%	3.6	29.5	35.3%	53.4%	7.4	26.5	39.5%
ToP	5	5	> 0	<b>87.1%</b>	<b>1.7</b>	<b>34.2</b>	<b>0.0%</b>	<b>93.3%</b>	<b>0.9</b>	<b>36.3</b>	<b>0.0%</b>	<b>88.3%</b>	<b>1.3</b>	<b>34.4</b>	<b>0.0%</b>
TAP-NET++	10	0	> 0	66.8%	3.6	20.6	24.8%	77.0%	2.1	26.6	18.9%	68.2%	3.0	21.2	23.5%
ToP	10	0	> 0	<b>88.8%</b>	<b>1.2</b>	<b>34.8</b>	<b>0.0%</b>	<b>95.0%</b>	<b>0.3</b>	<b>37.1</b>	<b>0.0%</b>	<b>89.1%</b>	<b>1.6</b>	<b>35.1</b>	<b>0.0%</b>

**Figure 10.** Asymptotic planning performance with space utilization labeled in each grid.**Table 9.** Performance comparisons on offline 3D-BPP.

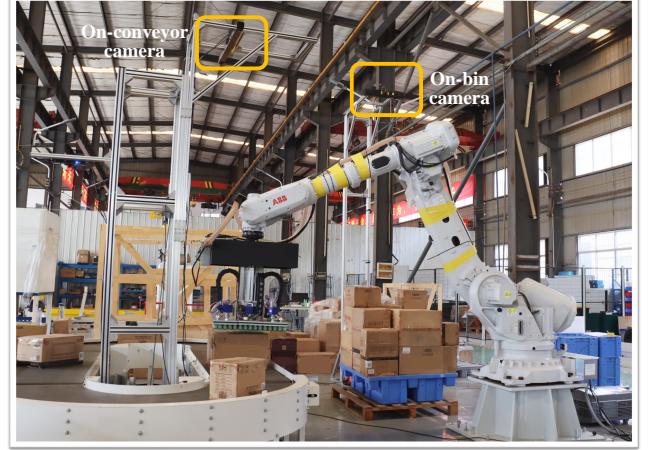
Method	Sel.	Prev.	Un.	Setting 2			
				Uti. $\uparrow$	Var. $\downarrow$	Num. $\uparrow$	Gap $\downarrow$
Gurobi	50	0	0	76.8%	11.5	29.9	19.3%
RCQL	50	0	0	77.8%	3.4	19.9	18.3%
Attend2Pack	50	0	0	87.6%	4.4	26.0	8.0%
TAP-NET++	50	0	0	89.2%	1.2	28.0	6.3%
ToP	50	0	0	<b>95.2%</b>	<b>0.2</b>	<b>36.3</b>	<b>0.0%</b>

on *setting 2*. The heatmap clearly reveals that, as decision variables increase, the packing performance also improves. Visualizations of ToP results across different BPP variations can be found in Appendix D.

We also compare ToP on the widely studied offline BPP (Martello et al. 2000), where  $s = |I|$  and  $p = u = 0$ . Baselines include the traditional optimization solver Gurobi (LLC Gurobi Optimization 2018) and learning-based methods including RCQL (Li et al. 2022), Attend2Pack (Zhang et al. 2021), and TAP-NET++ (Xu et al. 2023). The total number of items  $|I| = 50$ . Unlike online packing ( $u > 0$ ), where items arrive continuously and intermediate decisions must be made, offline packing allows iterative optimization for better solutions. To ensure fairness, each method’s decision time is capped at 600 seconds. The results, summarized in Table 9, illustrate that ToP outperforms all baselines. Traditional solvers often get stuck in local optima, leading to low-quality solutions within the time limit.

#### 4.7 Real-World Packing Robot

We develop a real-world packing robot in an industrial warehouse, as presented in Figure 11. The system adopts an ABB IRB 6700 robotic arm with a 210kg load capacity. Boxes (items) are delivered via a conveyor belt, which stops upon box detection by a photoelectric sensor. A key challenge for robotic packing is safely and efficiently placing boxes into constrained spaces where objects are positioned

**Figure 11.** Our real-world packing system. The on-conveyor camera detects targets. The on-bin one monitors possible drifts.

closely. Even minor robot-object collisions can destabilize the stack, leading to serious production failure. Moreover, unlike laboratory packing scenarios with protective container walls (Yang et al. 2021a; Xu et al. 2023), industrial packing often omits such protection for efficiency, making the constrained placement problem (Choset et al. 2005) more challenging. Solving it with motion planning (Görner et al. 2019) requires precise scene modeling and is time-consuming, violating practical demands.

Instead of motion planning, we adopt a simple top-down placement manner with a flexible modular gripper which can actively adjust its shape to satisfy constrained placements. Each module is equipped with multiple suction cups for gripping flat items. Modules vary in size, allowing the gripper to adjust its own shape based on the target box’s size, as illustrated in Figure 12 (a). The shape adjustment principle is simplified to maximize box coverage without exceeding the box’s top boundary, providing sufficient gripping force while avoiding robot-object collisions during placement, as demonstrated in Figure 12 (b) and (c). This ensures both efficiency and safety in industrial scenarios.

The warehouse stocks 8000 Stock Keeping Units (SKUs), including large-sized boxes ranging up to  $80 \times 80 \times 60$ cm, with a maximum weight of 30kg. The unprotected pallet measures  $120 \times 100$ cm, and the maximum stack height is 140cm. An RGB-D camera (PhoXi 3D Scanner XL) captures the top surface of incoming boxes. Item detection and segmentation are performed using Mask R-CNN (He et al. 2017), achieving a 99.95% recognition success rate for boxes on the conveyor. The modular gripper consists of 165 suction cups (39mm diameter), adjustable via a rodless pneumatic cylinder, with a maximum suction force of  $260\text{kg}/\text{m}^2$ . It automatically adjusts its configuration while approaching the

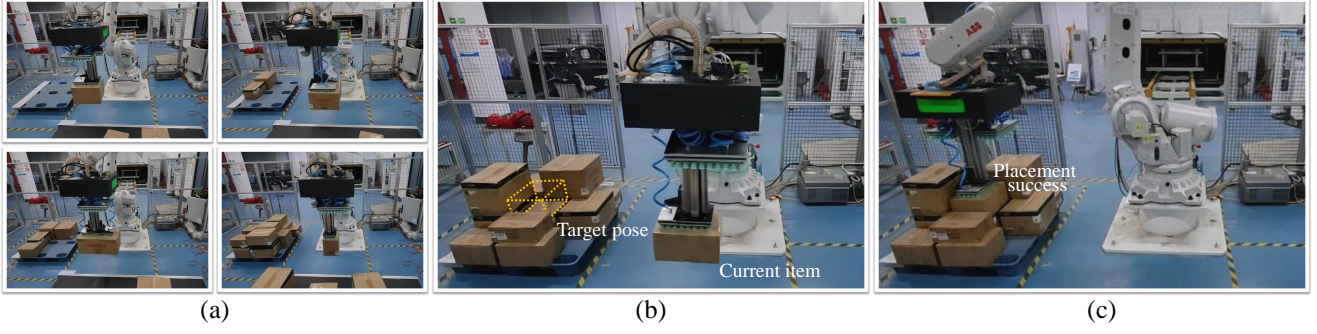


**Figure 12.** (a) The gripper actively adjusts its shape to adapt to the constrained placement requirements. (b) The robot grips and transfers boxes to the target pose where the surrounded boxes exist. Oversized end-effectors may cause collisions with placed boxes. (c) Our modular gripper dynamically adapts its shape to achieve constrained placement.



**Figure 13.** Transportation of packed boxes in a warehouse.

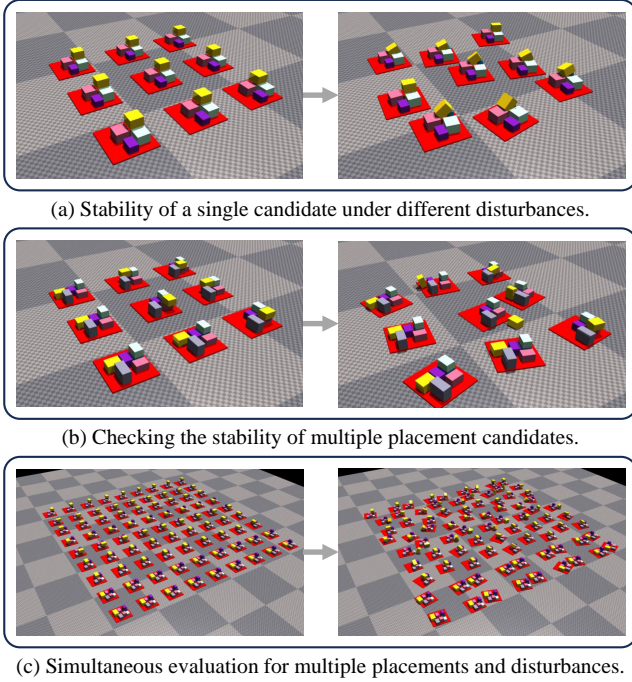


**Figure 14.** Simultaneously sampling multiple disturbances to simulate the real-world dynamic transportation.

target box, ensuring no delay in the packing cycle. The gripper has a 40cm lifting stroke, so surrounding boxes must not exceed 40cm above the top surface of the target placement. Placement candidates violating this constraint are discarded.

Aside from constrained placement, another major challenge in industrial packing lies in ensuring the stability of packed boxes during dynamic transportation (Hof et al. 2005). As exhibited in Figure 13, packed boxes are moved by Automated Guided Vehicles (AGVs) or human workers, involving passive motions like lift, acceleration/deceleration, and rotation of the stack. Most existing

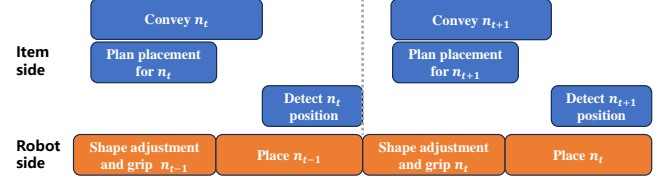


**Figure 15.** Our asynchronous packing pipeline. Blue blocks represent item-side operations, while orange blocks represent robot-side operations. This design ensures the robot is always prepared to pack the next box, maximizing efficiency.

packing research relies on quasi-static equilibrium for stability evaluation (Wang and Hauser 2019b; Zhao et al. 2022b), which does not hold under dynamic conditions.

We model real-world transportation uncertainties through physics-based verification. Ideally, if a real-world disturbance set  $d$  causes stack  $\mathbf{B}$  to collapse, a physical simulator  $\mathcal{E}$ , as  $\mathbf{B}$ 's digital twin, should predict this and reject unstable placements. However, real-world disturbances cannot be captured or recorded. To this, we randomly sample multiple disturbance sets to evaluate the stability for each placement, as illustrated in Figure 14 (a). Each disturbance set is a combination of 10 randomly generated translations and rotations, with translations in range [15, 20]cm along the  $x$  and  $y$  axes and rotations in range  $[-10^\circ, 10^\circ]$  for the  $z$  axis. The simulated linear and angular velocities are set to 6m/s and  $30^\circ/\text{s}$ , respectively. If any disturbance causes the stack to collapse, we consider a placement  $l$  unacceptable and turn to its alternatives (Figure 14 (b)). To meet real-time decision-making requirements of industrial packing, we leverage the Isaac Gym simulator (Makoviychuk et al. 2021), which feature batch parallelism and GPU-based simulation acceleration. For each placement, we sample  $k_d$  disturbance sets, and evaluate  $k_l$  such placements simultaneously, as exhibited in Figure 14 (c). We select the top  $k_l$  placements based on probabilities output by policy  $\pi_\theta$ .

A promising approach to leverage physics-based stability evaluation is to incorporate it as training guidance (e.g., serving as a reward signal), making the trained policies physics-aware and eliminating test-side simulation costs. However, we do not adopt this approach for two practical reasons. First, Isaac Gym's parallelism offers little benefit for online packing, which requires generating new objects and dynamically modifying the simulated scene—an expensive operation due to scene data being preloaded to CUDA memory and the high cost of CPU-GPU synchronization. Second, Zhao et al. (2021) find that purely relying on





**Figure 16.** Real-world packing experiments conducted on a warehouse scenario with a maximum buffer size of 3.

**Table 10.** Real-world transportation stability (%). Test-time evaluation are conducted with quasi-static equilibrium (Zhao et al. 2022b) and our physics-based verification. Each is evaluated with 20 packing episodes.

Quasi-Static Equilibrium	Ours ( $k_d = 1$ )	Ours ( $k_d = 2$ )	Ours ( $k_d = 4$ )	Ours ( $k_d = 8$ )
55%	70%	85%	95%	100.0%

training-side constraints inevitably leads to occasional packing instability during testing. Hence, we conclude that simulation for test-time stability evaluation is always necessary, whereas training can proceed without it. For encouraging physics awareness in the base PCT policy  $\pi_\theta$ , we incorporate the fast quasi-static equilibrium estimation method proposed by Zhao et al. (2022b) for training.

Even powered by batch parallelism and GPU-based acceleration, the test-time simulation inevitably increases computational costs and affects packing cycles/manufacturing throughputs. We propose an asynchronous decision pipeline for efficiency optimization. As presented in Figure 15, while the robot is packing box  $n_{t-1}$ , the system simultaneously prepares box  $n_t$  by transporting it on the conveyor, retrieving its dimensions from the central controller, calculating its placement and stability, and capturing RGB-D images for location detection. Since the robot-side execution cost cannot be optimized, we focus on minimizing the item-side computing time to ensure it is shorter than the robot execution time. This keeps the robot always ready to pack the next box, maximizing efficiency.

The conveyor can hold up to 3 boxes for the robot to grip, modeling the general setting of packing with  $1 \leq s \leq 3$  and  $0 \leq p \leq 2$ . We adopt ToP for solving different BPP variations out of the box. The task terminates when the stack reaches height limitation or no stable placement is available. AGVs or forklifts then transport the stack, and the packing restarts on a new pallet. During placement, the robot maintains a 1.5cm gap between each box. This is necessary due to the sensitivity of packing to operation accuracy.

After box  $n$  is placed, the RGB-D camera (HIKROBOT MV-DB1300A) on the pallet detects its position. If any deviation from the planned position is observed, the internal description of  $n$  is updated accordingly to inform subsequent placement decisions. The average packing cycle is 10 seconds per box. Without container protection, 363 packing episodes are conducted in real-world industrial production, packing 6891 boxes with an average of 19

boxes per pallet and a 57.4% space utilization for relatively large-size boxes. Throughout the packing production, no robot-object collisions occurred and no stacks collapsed during transportation. We summarize how our physics-aware randomization improves transportation stability in Table 10, and take the disturbance number  $k_d = 8$  for test-time stability evaluation. A visual example of real-world packing is shown in Figure 16, with additional results provided in Appendix D. A video showcasing the dynamic packing process—featuring active gripper adjustment and stable transportation, is included in Supplementary Material.

## 5 Conclusions and Discussions

We formulate the online 3D-BPP as a novel hierarchical representation—packing configuration tree (PCT). PCT is a full-fledged description of the state and action space of bin packing which makes the DRL agent easy to train and well-performing. We extract state features from PCT using graph attention networks which encode the spatial relations of all space configuration nodes. The graph representation of PCT helps the agent with handling online 3D-BPP with complex practical constraints, while the finite leaf nodes prevent the action space from growing explosively. We further discover the potential of PCT as a tree-based planner to deliberately solve packing problems of industrial significance, including large-scale packing and different BPP variations.

Our method surpasses all other online packing competitors and is the first learning-based method that solves online 3D-BPP with continuous solution space. It performs well even on item sampling distributions that are different from the training one. We also give demonstrations to prove that PCT is versatile in terms of incorporating various practical constraints. The PCT-driven planning excels across large problem scales and different BPP variations, with performance improving as the problem scales and decision variables increase. Our real-world packing robot operates reliably on unprotected pallets, densely packing at 10 seconds per box with an average of 19 boxes and a 57.4% space utilization for relatively large-size boxes.

**Limitation and future work** We see several important opportunities for future research. First, we use the default physical simulation parameters (Makoviychuk et al. 2021) to evaluate the stability of real-world packing, where the Sim2Real gap can lead to incorrect solutions being either discarded or retained. From both academic and industrial perspectives, we are highly interested in estimating physical parameters from real-world packing processes to achieve system identification, support more accurate stability evaluation and Real2Sim2Real packing policy learning (Li et al. 2025). Additionally, this work models items as rigid bodies. Exploring ways to incorporate the deformability of items or containers (Bahety et al. 2023) to achieve tighter packing would be an intriguing direction. Last but not least, this work expands the industrial applicability of PCT through planning approaches, with its capability still bounded by the pre-trained base model. Developing PCT as a foundation model (Firoozi et al. 2025) trained on diverse packing data, with zero-shot generalization to new packing scenarios, is an exciting and promising avenue for future research.

## References

- Bahety A, Jain S, Ha H, Hager N, Burchfiel B, Cousineau E, Feng S and Song S (2023) Bag all you need: Learning a generalizable bagging strategy for heterogeneous objects. In: *IEEE/RSJ International Conference on Intelligent Robots and Systems*.
- Bello I, Pham H, Le QV, Norouzi M and Bengio S (2017) Neural combinatorial optimization with reinforcement learning. In: *International Conference on Learning Representations*.
- Bruna J, Zaremba W, Szlam A and LeCun Y (2014) Spectral networks and locally connected networks on graphs. In: *International Conference on Learning Representations*.
- Choset H, Lynch KM, Hutchinson S, Kantor GA and Burgard W (2005) *Principles of robot motion: theory, algorithms, and implementations*. MIT press.
- Coumans E and Bai Y (2016) Pybullet, a python module for physics simulation for games, robotics and machine learning. URL <http://pybullet.org>.
- Crainic TG, Perboli G and Tadei R (2008) Extreme point-based heuristics for three-dimensional bin packing. *INFORMS Journal on Computing*.
- Crainic TG, Perboli G and Tadei R (2009) Ts2pack: A two-level tabu search for the three-dimensional bin packing problem. *European Journal of Operational Research*.
- De Castro Silva J, Soma N and Maculan N (2003) A greedy search for the three-dimensional bin packing problem: the packing static stability case. *International Transactions in Operational Research*.
- Demisse G, Mihalyi R, Okal B, Poudel D, Schauer J and Nüchter A (2012) Mixed palletizing and task completion for virtual warehouses. In: *Virtual Manufacturing and Automation Competition Workshop at the International Conference of Robotics and Automation*.
- Dijkstra EW (2022) A note on two problems in connexion with graphs. In: *Edsger Wybe Dijkstra: His Life, Work, and Legacy*.
- Duan L, Hu H, Qian Y, Gong Y, Zhang X, Wei J and Xu Y (2019) A multi-task selected learning approach for solving 3D flexible bin packing problem. In: *International Conference on Autonomous Agents and MultiAgent Systems*.
- Egeblad J, Nielsen BK and Odgaard A (2007) Fast neighborhood search for two-and three-dimensional nesting problems. *European Journal of Operational Research*.
- Faroe O, Pisinger D and Zachariassen M (2003) Guided local search for the three-dimensional bin-packing problem. *INFORMS Journal on Computing*.
- Firoozi R, Tucker J, Tian S, Majumdar A, Sun J, Liu W, Zhu Y, Song S, Kapoor A, Hausman K, Ichter B, Driess D, Wu J, Lu C and Schwager M (2025) Foundation models in robotics: Applications, challenges, and the future. *The International Journal of Robotics Research*.
- Gori M, Monfardini G and Scarselli F (2005) A new model for learning in graph domains. In: *Proceedings. 2005 IEEE International Joint Conference on Neural Networks, 2005*.
- Görner M, Haschke R, Ritter H and Zhang J (2019) Moveit! task constructor for task-level motion planning. In: *International Conference on Robotics and Automation*.
- Grove EF (1995) Online bin packing with lookahead. In: *Annual ACM-SIAM Symposium on Discrete Algorithms*.
- Gzara F, Elhedhli S and Yildiz BC (2020) The pallet loading problem: Three-dimensional bin packing with practical constraints. *European Journal of Operational Research*.
- Ha CT, Nguyen TT, Bui LT and Wang R (2017) An online packing heuristic for the three-dimensional container loading problem in dynamic environments and the physical internet. In: *Applications of Evolutionary Computation*.
- Haarnoja T, Zhou A, Abbeel P and Levine S (2018) Soft actor-critic: Off-policy maximum entropy deep reinforcement learning with a stochastic actor. In: *International Conference on Machine Learning*.
- Hart PE, Nilsson NJ and Raphael B (1968) A formal basis for the heuristic determination of minimum cost paths. *Transactions on Systems Science and Cybernetics*.
- He K, Gkioxari G, Dollár P and Girshick RB (2017) Mask R-CNN. In: *IEEE International Conference on Computer Vision*.
- Hof AL, Gazendam M and Sinke W (2005) The condition for dynamic stability. *Journal of Biomechanics*.
- Hong Y, Kim Y and Lee K (2020) Smart pack: Online autonomous object-packing system using RGB-D sensor data. *Sensors*.
- Hu H, Zhang X, Yan X, Wang L and Xu Y (2017) Solving a new 3D bin packing problem with deep reinforcement learning method. *arXiv preprint arXiv:1708.05930*.
- Hu R, Xu J, Chen B, Gong M, Zhang H and Huang H (2020) Tap-net: transport-and-pack using reinforcement learning. *ACM Transactions on Graphics*.
- Kagerer F, Beinhofer M, Stricker S and Nüchter A (2023) Bed-bpp: Benchmarking dataset for robotic bin packing problems. *The International Journal of Robotics Research*.
- Kang K, Moon I and Wang H (2012) A hybrid genetic algorithm with a new packing strategy for the three-dimensional bin packing problem. *Applied Mathematics and Computation*.
- Karabulut K and Inceoglu MM (2004) A hybrid genetic algorithm for packing in 3D with deepest bottom left with fill method. In: *Advances in Information Systems*.
- Kool W, van Hoof H and Welling M (2019) Attention, learn to solve routing problems! In: *International Conference on Learning Representations*.
- Korf RE (1998) A complete anytime algorithm for number partitioning. *Artificial Intelligence*.
- Li D, Gu Z, Wang Y, Ren C and Lau FC (2022) One model packs thousands of items with recurrent conditional query learning. *Knowledge-Based Systems*.
- Li W, Zhao H, Yu Z, Du Y, Zou Q, Hu R and Xu K (2025) Pin-wm: Learning physics-informed world models for non-prehensile manipulation. In: *Robotics: Science and Systems*.
- Liu S, Wang S, Zhang P, Xu K, Liu X, Zhang C and Gao F (2022) Efficient one-pass multi-view subspace clustering with consensus anchors. In: *AAAI Conference on Artificial Intelligence*.
- LLC Gurobi Optimization (2018) Gurobi optimizer reference manual. <https://tinyurl.com/4uxkx7nw>.
- Makoviychuk V, Wawrzyniak L, Guo Y, Lu M, Storey K, Macklin M, Hoeller D, Rudin N, Allshire A, Handa A and State G (2021) Isaac gym: High performance gpu-based physics simulation for robot learning. *arXiv preprint arXiv:2108.10470*.
- Martello S, Pisinger D and Vigo D (2000) The three-dimensional bin packing problem. *Operations Research*.
- Martello S, Pisinger D, Vigo D, Boef ED and Korst J (2007) Algorithm 864: General and robot-packable variants of the



- three-dimensional bin packing problem. *ACM Transactions on Mathematical Software* .
- Martens J and Grosse RB (2015) Optimizing neural networks with kronecker-factored approximate curvature. In: *International Conference on Machine Learning*.
- Mayne DQ, Rawlings JB, Rao CV and Scokaert PO (2000) Constrained model predictive control: Stability and optimality. *Automatica* .
- Newell A, Shaw JC and Simon HA (1959) Report on a general problem solving program. In: *IFIP Congress*.
- Page A (1981) The biaxial compressive strength of brick masonry. *Proceedings of the Institution of Civil Engineers* .
- Pan JH, Hui KH, Gao X, Zhu S, Liu YH, Heng PA and Fu CW (2023a) Sdf-pack: Towards compact bin packing with signed-distance-field minimization. In: *IEEE/RSJ International Conference on Intelligent Robots and Systems*.
- Pan Y, Chen Y and Lin F (2023b) Adjustable robust reinforcement learning for online 3D bin packing. *Advances in Neural Information Processing Systems* .
- Puche AV and Lee S (2022) Online 3D bin packing reinforcement learning solution with buffer. In: *IEEE/RSJ International Conference on Intelligent Robots and Systems*.
- Qi CR, Su H, Mo K and Guibas LJ (2017) Pointnet: Deep learning on point sets for 3D classification and segmentation. In: *IEEE Conference on Computer Vision and Pattern Recognition*.
- Qiu R, Sun Z and Yang Y (2022) Dimes: A differentiable meta solver for combinatorial optimization problems. *Advances in Neural Information Processing Systems* 35.
- Ramos AG, Oliveira JF and Lopes MP (2016) A physical packing sequence algorithm for the container loading problem with static mechanical equilibrium conditions. *International Transactions in Operational Research* .
- Seiden SS (2002) On the online bin packing problem. *Journal of the ACM* .
- Shin HV, Porst CF, Vouga E, Ochsendorf J and Durand F (2016) Reconciling elastic and equilibrium methods for static analysis. *ACM Transactions on Graphics* .
- Silver D, Huang A, Maddison CJ, Guez A, Sifre L, van den Driessche G, Schrittwieser J, Antonoglou I, Panneershelvam V, Lanctot M, Dieleman S, Grewe D, Nham J, Kalchbrenner N, Sutskever I, Lillicrap TP, Leach M, Kavukcuoglu K, Graepel T and Hassabis D (2016) Mastering the game of Go with deep neural networks and tree search. *Nature* .
- Silver D, Schrittwieser J, Simonyan K, Antonoglou I, Huang A, Guez A, Hubert T, Baker L, Lai M, Bolton A, Chen Y, Lillicrap TP, Hui F, Sifre L, van den Driessche G, Graepel T and Hassabis D (2017) Mastering the game of go without human knowledge. *Nature* .
- Sim4Dexterity (2023) ICRA 2023 virtual manipulation challenge: Stacking. <https://tinyurl.com/4asfdnex>.
- Spaan MT (2012) Partially observable markov decision processes. In: *Reinforcement Learning: State-of-the-Art*. Springer.
- Sun Z and Yang Y (2023) DIFUSCO: graph-based diffusion solvers for combinatorial optimization. In: *Advances in Neural Information Processing Systems*.
- Sutton RS and Barto AG (2018) *Reinforcement Learning: An Introduction*. MIT press.
- Taylor ME and Stone P (2009) Transfer learning for reinforcement learning domains: A survey. *Journal of Machine Learning Research* .
- Vaswani A, Shazeer N, Parmar N, Uszkoreit J, Jones L, Gomez AN, Kaiser L and Polosukhin I (2017) Attention is all you need. In: *Advances in Neural Information Processing Systems*.
- Velickovic P, Cucurull G, Casanova A, Romero A, Liò P and Bengio Y (2018) Graph attention networks. In: *International Conference on Learning Representations*.
- Verma R, Singhal A, Khadilkar H, Basumatary A, Nayak S, Singh HV, Kumar S and Sinha R (2020) A generalized reinforcement learning algorithm for online 3D bin-packing. *arXiv preprint arXiv:2007.00463* .
- Vinyals O, Fortunato M and Jaitly N (2015) Pointer networks. In: *Advances in Neural Information Processing Systems*.
- Wang F and Hauser K (2019a) Robot packing with known items and nondeterministic arrival order. In: *Robotics: Science and Systems*.
- Wang F and Hauser K (2019b) Stable bin packing of non-convex 3D objects with a robot manipulator. In: *International Conference on Robotics and Automation*.
- Wang F and Hauser K (2021) Dense robotic packing of irregular and novel 3D objects. *IEEE Transactions on Robotics* .
- Wu Y, Mansimov E, Grosse RB, Liao S and Ba J (2017) Scalable trust-region method for deep reinforcement learning using kronecker-factored approximation. In: *Advances in Neural Information Processing Systems*.
- Xu J, Gong M, Zhang H, Huang H and Hu R (2023) Neural packing: from visual sensing to reinforcement learning. *ACM Transactions on Graphics* .
- Yang Z, Yang S, Song S, Zhang W, Song R, Cheng J and Li Y (2021a) Packerbot: Variable-sized product packing with heuristic deep reinforcement learning. In: *International Conference on Intelligent Robots and Systems*.
- Yang Z, Yang S, Song S, Zhang W, Song R, Cheng J and Li Y (2021b) Packerbot: Variable-sized product packing with heuristic deep reinforcement learning. In: *IEEE/RSJ International Conference on Intelligent Robots and Systems*.
- Yu K, Zhao H, Huang Y, Yi R, Xu K and Zhu C (2024) Disco: Efficient diffusion solver for large-scale combinatorial optimization problems. *arXiv preprint arXiv:2406.19705* .
- Yuan J, Zhang J, Cai Z and Yan J (2023) Towards variance reduction for reinforcement learning of industrial decision-making tasks: A bi-critic based demand-constraint decoupling approach. In: *ACM SIGKDD Conference on Knowledge Discovery and Data Mining*.
- Zhang J, Zi B and Ge X (2021) Attend2pack: Bin packing through deep reinforcement learning with attention. *arXiv preprint arXiv:2107.04333* .
- Zhao H, Pan Z, Yu Y and Xu K (2023) Learning physically realizable skills for online packing of general 3D shapes. *ACM Transactions on Graphics* .
- Zhao H, She Q, Zhu C, Yang Y and Xu K (2021) Online 3D bin packing with constrained deep reinforcement learning. In: *AAAI Conference on Artificial Intelligence*.
- Zhao H, Yu Y and Xu K (2022a) Learning efficient online 3D bin packing on packing configuration trees. In: *International Conference on Learning Representations*.
- Zhao H, Zhu C, Xu X, Huang H and Xu K (2022b) Learning practically feasible policies for online 3D bin packing. *Science China Information Sciences* .

## Appendix

In this appendix, we provide more details and statistical results of our PCT method. Our real-world packing demo is also submitted with the supplemental material.

### A Implementation Details

**Deep Reinforcement Learning** We formulate online 3D-BPP as a Markov Decision Process and solve it with the deep reinforcement learning method. A DRL agent seeks a policy  $\pi$  to maximize the accumulated discounted reward:

$$J(\pi) = E_{\tau \sim \pi} \left[ \sum_{t=0}^{\infty} \gamma^t R(s_t, a_t) \right] \quad (12)$$

Where  $\gamma \in [0, 1]$  is the discount factor, and  $\tau = (s_0, a_0, s_1, \dots)$  is a trajectory sampled based on the policy  $\pi$ . We extract the feature of state  $s_t = (\mathcal{T}_t, n_t)$  using graph attention networks (Velickovic et al. 2018) for encoding the spatial relations of all space configuration nodes. The context feature is fed to two key components of our pipeline: an actor network and a critic network. The actor network, designed based on a pointer mechanism, weighs the leaf nodes of PCT, which is written as  $\pi(a_t|s_t)$ . The action  $a_t$  is an index of selected leaf node  $l \in \mathbf{L}_t$ , denoted as  $a_t = \text{index}(l)$ . The critic network maps the context feature into a state value prediction  $V(s_t)$ , which helps the training of the actor network. The whole network is trained via a composite loss  $L = \alpha \cdot L_{actor} + \beta \cdot L_{critic}$  ( $\alpha = \beta = 1$  in our implementation), which consists of actor loss  $L_{actor}$  and critic loss  $L_{critic}$ . These two loss functions are defined as:

$$\begin{aligned} L_{actor} &= (r_t + \gamma V(s_{t+1}) - V(s_t)) \log \pi(a_t|s_t) \\ L_{critic} &= (r_t + \gamma V(s_{t+1}) - V(s_t))^2 \end{aligned} \quad (13)$$

Where  $r_t = c_r \cdot w_t$  is our reward signal, and we set  $\gamma$  as 1 since the packing episode is finite. We adopt a step-wise reward  $r_t = c_r \cdot w_t$  once  $n_t$  is inserted into PCT as an internal node successfully. Otherwise,  $r_t = 0$  and the packing episode ends. The choice of item weight  $w_t$  depends on the packing preferences. In the general sense, we set  $w_t$  as the volume occupancy  $v_t = s_n^x \cdot s_n^y \cdot s_n^z$  of  $n_t$ , and the constant  $c_r$  is  $10/(S^x \cdot S^y \cdot S^z)$ . For online 3D-BPP with additional packing constraints, this weight can be set as  $w_t = \max(0, v_t - c \cdot O(s_t, a_t))$ . While the term  $v_t$  ensures that space utilization is still the primary concern, the objective function  $O(s_t, a_t)$  guides the agent to satisfy additional constraints like isle friendliness and load balancing. We adopt the ACKTR (Wu et al. 2017) method for training our DRL agent, which iteratively updates an actor and a critic using Kronecker-factored approximate curvature (K-FAC) (Martens and Grosse 2015) with trust region. Zhao et al. (2021) have demonstrated that this method has a surprising superiority on online 3D packing problems over other model-free DRL algorithms like SAC (Haarnoja et al. 2018).

**Feature extraction** Specifically, ACKTR runs multiple parallel processes (64 here) to interact with their respective environments and gather samples. The different processes may have different packing time steps  $t$  and deal with different packing sequences; the space configuration node

number  $N$  also changes. To combine these data with irregular shapes into one batch, we fulfill  $\mathbf{B}_t$  and  $\mathbf{L}_t$  to fixed lengths,  $80$  and  $25 \cdot |\mathbf{O}|$  respectively, with dummy nodes. The descriptors for dummy nodes are all-zero vectors and have the same size as the internal nodes or the leaf nodes. The relation weight logits  $u_{ij}$  of dummy node  $j$  to arbitrary node  $i$  is replaced with  $-\text{inf}$  to eliminate these dummy nodes during the feature calculation of GAT. The global context feature  $\bar{h}$  is aggregated only on the eligible nodes  $\mathbf{h}$ :  $\bar{h} = \frac{1}{N} \sum_{i=1}^N h_i$ . All space configuration nodes are embedded by GAT as a fully connected graph as Figure 2 (b), without any inner mask operation.

We only provide the packable leaf nodes that satisfy placement constraints for DRL agents. For *setting 2*, we check in advance if a candidate placement satisfies Constraints 2 and 3. For *setting 1* and *setting 3*, where the mass of item  $n_t$  is  $v_t$  and  $\rho \cdot v_t$  respectively, we will additionally check if one placement meets the constraints of packing stability. Benefits from the fast stability estimation method proposed by Zhao et al. (2022b), this pre-checking process can be completed in a very short time, and our DRL agent samples data at a frequency of more than 400 FPS.

The node-wise MLPs  $\phi_{\theta_B}$ ,  $\phi_{\theta_L}$ , and  $\phi_{\theta_n}$  used to embed raw space configuration nodes are two-layer linear networks with LeakyReLU activation function.  $\phi_{FF}$  is a two-layer linear structure activated by ReLU. The feature dimensions  $d_h, d_k$ , and  $d_v$  are 64. The hyperparameter  $c_{clip}$  used to control the range of clipped compatibility logits is set to 10 in our GAT implementation.

**Choice of PCT Length** Since PCT allows discarding some valid leaf nodes and this will not harm our performance, we randomly intercept a subset  $\mathbf{L}_{sub_t}$  from  $\mathbf{L}_t$  if  $|\mathbf{L}_t|$  exceeds a certain length. Determining the suitable PCT length for different bin configurations is important, we give our recommendations for finding this hyperparameter. For training, we find that the performance of learned policies is more sensitive to the number of allowed orientations  $|\mathbf{O}|$ . Thus we set the PCT length as  $c \cdot |\mathbf{O}|$  where  $c$  can be determined by a grid search nearby  $c = 25$  for different bin configurations. For our experiments,  $c = 25$  works quite well. During the test, the PCT length can be different from the training one, we suggest searching for this interception length with a validation dataset via a grid search, which ranges from 50 to 300 with a step length of 10.

### B Leaf Node Expansion Schemes

We introduce the leaf node expansion schemes adopted in our PCT implementation here. These schemes are used to incrementally calculate new candidate placements introduced by the just-placed item  $n_t$ . A good expansion scheme should reduce the number of solutions to be explored while not missing too many feasible packings. Meanwhile, polynomials computability is also expected. As shown in Figure 17, the policies guided by suitable leaf node expansion schemes outperform the policy trained on a full coordinate (FC) space in the whole training process. We extend three existing heuristic placement rules, which have proven to be both accurate and efficient, to our PCT expansion, i.e. *Corner Point*, *Extreme Point*, and *Empty Maximal Space*. Since all these schemes are related to

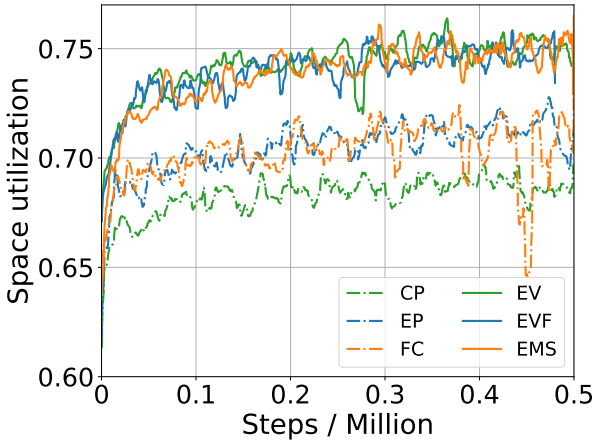


**Figure 17.** Learning curves on *setting 1*. A good expansion scheme for PCT reduces the complexity and helps DRL methods for more efficient learning and better performance. EVF means the full EV leaf node set without an interception.

boundary points of packed items, we combine the start/end points of  $n_t$  with these boundary points as a superset, namely *Event Point*.

**Corner Point** Martello et al. (2000) first introduce the concept of Corner Point (CP) for their branch-and-bound methods. Given 2D packed items in the  $xoy$  plane, the corner points can be found where the envelope of the items in the bin changes from vertical to horizontal, as shown in Figure 18 (a). The past corner points that no longer meet this condition will be deleted.

Extend this 2D situation to 3D cases, the new candidate 3D positions introduced by the just placed item  $n_t$  are a subset of  $\{(p_n^x + s_n^x, p_n^y, p_n^z), (p_n^x, p_n^y + s_n^y, p_n^z), (p_n^x, p_n^y, p_n^z + s_n^z)\}$  if the envelope of the corresponding 2D plane, i.e.  $xoy$ ,  $yozy$ , and  $xoz$ , is changed by  $n_t$ . The time complexity of finding 3D corner points incrementally is  $O(c)$  with an easy-to-maintained bin height map data structure to detect the change of envelope on each plane,  $c$  is a constant here.

**Extreme Point** Crainic et al. (2008) extend the concept of Corner Point to Extreme Point (EP) and claim their method reaches the best offline performance of that era. Its insight is to provide the means to exploit the free space defined inside a packing by the shapes of the items that already exist. When the current item  $n_t$  is added, new EPs are incrementally generated by projecting the coordinates  $\{(p_n^x + s_n^x, p_n^y, p_n^z), (p_n^x, p_n^y + s_n^y, p_n^z), (p_n^x, p_n^y, p_n^z + s_n^z)\}$  on the orthogonal axes, e.g., project  $(p_n^x + s_n^x, p_n^y, p_n^z)$  in the directions of the  $y$  and  $z$  axes to find intersections with all items lying between item  $n_t$  and the boundary of the bin. The nearest intersection in the respective direction is an extreme point. Since we stipulate a vertical top-down loading direction, the 3D extreme points in the strict sense may exist a large item blocking the loading direction. So we find the 2D extreme points (see Figure 18 (b)) in the  $xoy$  plane and repeat this operation on each distinct  $p^z$  value (i.e. start/end  $z$  coordinate of a packed item) which satisfies  $p_n^z \leq p^z \leq p_n^z + s_n^z$ . The time complexity of this method is  $O(m \cdot |B_{2D}|)$ , where  $B_{2D}$  is the packed items that exist in the corresponding  $z$  plane and  $m$  is the number of related  $z$  scans.

**Empty Maximal Space** Empty Maximal Spaces (EMSs) (Ha et al. 2017) are the largest empty orthogonal spaces whose sizes cannot extend more along the coordinate axes from their front-left-bottom (FLB) corner. This is a simple and effective placement rule. An EMS  $e$  is presented by its FLB corner  $(p_e^x, p_e^y, p_e^z)$  and sizes  $(s_e^x, s_e^y, s_e^z)$ . When the current item  $n_t$  is placed into  $e$  on its FLB corner, this EMS is split into three smaller EMSs with positions  $(p_e^x + s_n^x, p_e^y, p_e^z)$ ,  $(p_e^x, p_e^y + s_n^y, p_e^z)$ ,  $(p_e^x, p_e^y, p_e^z + s_n^z)$  and sizes  $(s_e^x - s_n^x, s_e^y, s_e^z)$ ,  $(s_e^x, s_e^y - s_n^y, s_e^z)$ ,  $(s_e^x, s_e^y, s_e^z - s_n^z)$ , respectively. If the item  $n_t$  only partially intersects with  $e$ , we can apply a similar volume subtraction to the intersecting part for splitting  $e$ . For each ems, we define the left-up  $(p_e^x, p_e^y + s_e^y, p_e^z)$ , right-up  $(p_e^x + s_e^x, p_e^y + s_e^y, p_e^z)$ , left-bottom  $(p_e^x, p_e^y, p_e^z)$ , and right-bottom  $(p_e^x + s_e^x, p_e^y, p_e^z)$  corners of its vertical bottom as candidate positions, as shown in Figure 18 (c). These positions also need to be converted to the FLB corner coordinate for placing item  $n_t$ . The left-up, right-up, left-bottom, and right-bottom corners of  $e$  should be converted to  $(p_e^x, p_e^y + s_e^y - s_n^y, p_e^z)$ ,  $(p_e^x + s_e^x - s_n^x, p_e^y + s_e^y - s_n^y, p_e^z)$ ,  $(p_e^x, p_e^y, p_e^z)$ , and  $(p_e^x + s_e^x - s_n^x, p_e^y, p_e^z)$  respectively. Since all EMSs  $e \in \mathbf{E}$  in the bin need to detect intersection with  $n_t$ , the time complexity of finding 3D EMSs incrementally is  $O(|\mathbf{E}|)$ . A 3D schematic diagram of PCT expansion guided by EMSs is provided in Figure 19.

**Event Point** It's not difficult to find that all schemes mentioned above are related to boundary points of a packed item along  $d \in \{x, y\}$  axes (we assume the initial empty bin is also a special packed item here). When the current item  $n_t$  is packed, we update the existing PCT leaf nodes by scanning all distinct  $p^z$  values that satisfy  $p_n^z \leq p^z \leq p_n^z + s_n^z$  and combine the start/end points of  $n_t$  with the boundary points that exist in this  $z$  plane to get the superset (see Figure 18 (d)), which is called *Event Points*. The time complexity for detecting event points is  $O(m \cdot |B_{2D}|^2)$ .

## C More Results

In this section, we report more results of our method. Section C.1 further discusses the generalization ability of our method on disturbed item sampling distributions and unseen items. Section C.2 visualizes packing sequences to analyze model behaviors. Section C.4 reports the running cost of each method. More visualized results are provided in Section D.

### C.1 Generalization Performance

The generalization ability of learning-based methods has always been a concern. Here we demonstrate that our method has a good generalization performance on item size distributions different from the training one. We conduct this experiment with continuous solution space. We sample item size  $s^d$  from normal distributions  $N(\mu, \sigma^2)$  for generating test sequences where  $\mu$  and  $\sigma$  are the expectation and the standard deviation. Three normal distributions are adopted here, namely  $N(0.3, 0.1^2)$ ,  $N(0.1, 0.2^2)$ , and  $N(0.5, 0.2^2)$ , as shown in Figure 20. The larger  $\mu$  of the normal distribution, the larger the average size of sampled items. We still control  $s^d$  within the range of  $[0.1, 0.5]$ . If the sampled item sizes are not within this range, we will resample until they meet the condition.

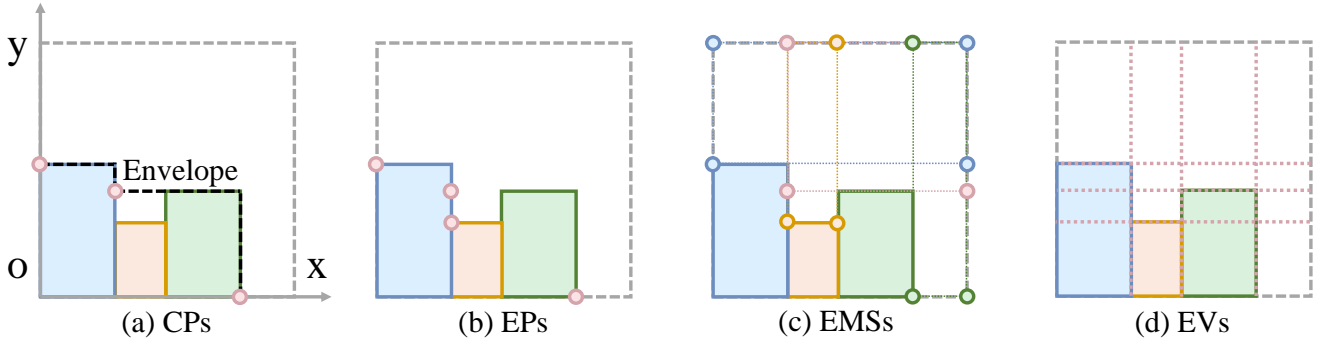


**Figure 18.** Full candidate positions generated by different PCT expansion schemes (all in  $xoy$  plane). The gray dashed lines are the boundaries of the bin. Circles in (a) and (b) represent corner points and extreme points, respectively. (c) The candidate positions (circles) introduced by different EMSs are rendered with different colors. All intersections of two dashed lines in (d) constitute event points.

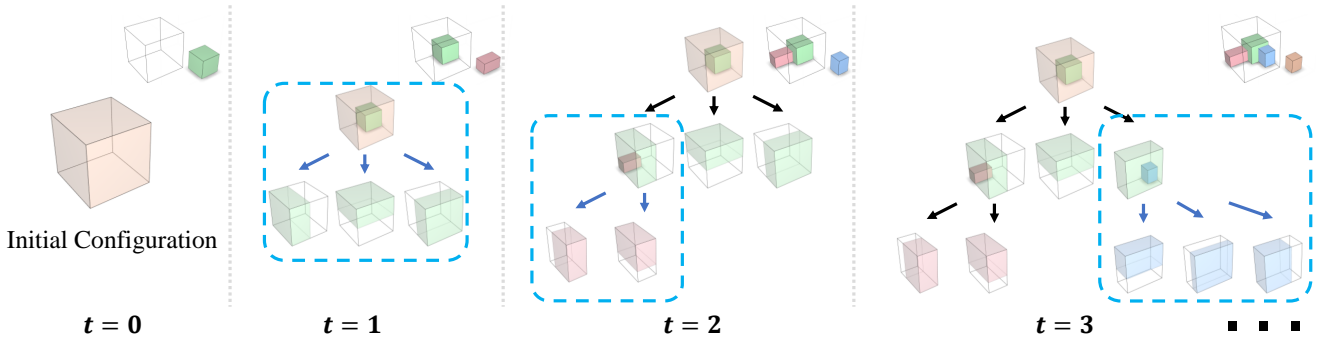


**Figure 19.** A 3D PCT expansion schematic diagram. This PCT grows under the guidance of the EMS expansion scheme. For simplicity, we only choose the bottom-right-up corners of each EMS as candidate positions, and we set  $|\mathbf{O}| = 1$  here.

**Table 11.** Generalization performance on different kinds of item sampling distributions.

Test Distribution	Method	Setting 1			Setting 2			Setting 3		
		Util. $\uparrow$	Var. $\downarrow$	Num. $\uparrow$	Util. $\uparrow$	Var. $\downarrow$	Num. $\uparrow$	Util. $\uparrow$	Var. $\downarrow$	Num. $\uparrow$
$s^d \sim U(0.1, 0.5)$	LSAH	48.3%	12.1	18.7	58.7%	4.6	22.8	48.4%	12.2	18.8
	PCT & EMS	65.3%	4.4	24.9	<b>66.3%</b>	<b>2.3</b>	<b>27.0</b>	<b>66.6%</b>	<b>3.3</b>	<b>25.3</b>
	PCT & EV	<b>65.4%</b>	<b>3.3</b>	<b>25.0</b>	65.0%	2.6	26.4	65.8%	3.6	25.1
$s^d \sim N(0.3, 0.1^2)$	LSAH	49.2%	11.1	18.9	60.0%	4.1	22.9	49.2%	11.0	18.9
	PCT & EMS	<b>66.1%</b>	3.6	<b>25.1</b>	<b>64.3%</b>	3.5	<b>25.6</b>	<b>66.4%</b>	3.0	<b>25.2</b>
	PCT & EV	65.1%	<b>2.8</b>	24.7	63.7%	<b>2.6</b>	25.3	66.2%	<b>2.9</b>	25.1
$s^d \sim N(0.1, 0.2^2)$	LSAH	52.4%	8.9	30.3	62.9%	<b>2.4</b>	44.3	52.3%	8.9	30.2
	PCT & EMS	<b>68.5%</b>	<b>2.5</b>	<b>39.0</b>	<b>66.4%</b>	3.0	<b>49.7</b>	<b>69.2%</b>	2.5	<b>39.4</b>
	PCT & EV	66.5%	2.7	38.0	64.9%	2.7	48.3	67.4%	<b>2.4</b>	38.5
$s^d \sim N(0.5, 0.2^2)$	LSAH	47.3%	12.6	13.0	56.0%	5.5	12.9	47.3%	12.6	13.0
	PCT & EMS	63.5%	5.0	17.3	<b>64.5%</b>	<b>2.8</b>	<b>15.4</b>	<b>65.2%</b>	3.8	<b>17.7</b>
	PCT & EV	<b>65.1%</b>	<b>3.3</b>	<b>17.7</b>	64.5%	2.8	15.3	65.1%	<b>3.7</b>	17.7

We directly transfer our policies trained on  $U(0.1, 0.5)$  to these new datasets without any fine-tuning. We use the best-performing heuristic method LSAH (Hu et al. 2017) in Section 4.3 as a baseline. The test results are summarized in Table 11. Our method performs well on distributions different from the training one and always surpasses the LSAH method. See Appendix C for more results about the generalization ability of our method on disturbed distributions and unseen items.

We demonstrate that our algorithm has a good generalization performance on disturbed item transitions, i.e.,  $\mathcal{P}(s_{t+1}|s_t)$ . Generalizing to a new transition is a classic challenge for reinforcement learning (Taylor and Stone 2009; Liu et al. 2022). We conduct this experiment in the discrete setting where the item set is finite ( $|I| = 125$ ). For each item  $n \in I$ , we add a random non-zero disturbance  $\delta_i$  on its original sample probability  $p_i$ , e.g.,  $p_i = p_i \cdot (1 - \delta_i)$ . We



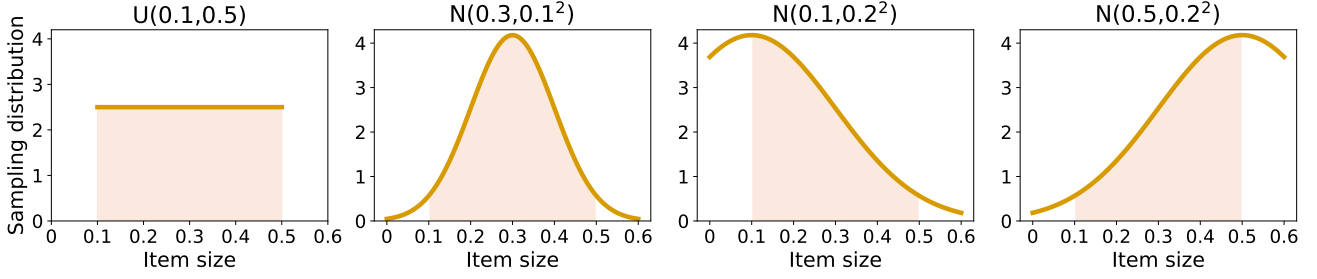


**Figure 20.** The probability distribution for sampling item sizes. The area of the colored zone is normalized to 1.

normalize the disturbed  $p_i$  as the final item sampling probability. Note that  $\delta_i$  is fixed during sampling one complete sequence. We test different ranges of  $\delta_i$  and the results are summarized in Table 12.

Benefits from the efficient guidance of heuristic leaf node expansion schemes, our method maintains its performance under various amplitude disturbances. Our method even behaves well with a strong disturbance  $\delta_i \in [-100\%, 100\%]$  applied, which means some items may never be sampled by some distributions when  $\delta_i = 1$  and  $p_i \cdot (1 - \delta_i) = 0$  in a specific sequence.

Beyond experiments on generalization to disturbed distributions, we also test our method with unseen items. We conduct this experiment in the discrete setting. We randomly delete 25 items from  $\mathcal{I}$  and train PCT policies with  $|\mathcal{I}_{sub}| = 100$ . Then we test the trained policies on full  $\mathcal{I}$ . See Table 13 for results. Our method still performs well on datasets where unseen items exist regarding all settings.

## C.2 Understanding of Model Behaviors

The qualitative understanding of model behaviors is important, especially for practical concerns. We visualize our packing sequences to give our analysis. The behaviors of learned models differ with the packing constraints. If there is no specific packing preference, our learned policies will start packing near a fixed corner (Figure 21 (a)). The learned policies tend to combine items of different heights together to form a plane for supporting future ones (Figure 21 (b)). Meanwhile, it prefers to assign little items to gaps and make room (Figure 21 (c)) for future large ones (Figure 21 (d)). If additional packing preference is considered, the learned policies behave differently. For online 3D-BPP with load balancing, the model will keep the maximum height in the bin as low as possible and pack items layer by layer (Figure 21(e)). For online 3D-BPP with isle friendliness, our model tends to pack the same category of items near the same bin corner (Figure 21 (f)).

## C.3 Performance on ICRA Stacking Challenge

The IEEE International Conference on Robotics and Automation (ICRA) organized the Stacking Challenge in 2023 (Sim4Dexterity 2023). This competition primarily focuses on packing problem variants with  $u > 0$ , including online packing problems with  $p = s = 1$ , forward-looking packing problems with  $p > s = 1$ , and general packing problems with  $p > s > 1$ . The bin dimensions are set to  $S_x = 2.141$ ,  $S_y = 1.076$ ,  $S_z = 0.99$ .

As shown in Figure 22, the item dimensions follow normal distributions: length  $s_x \sim \mathcal{N}(0.45, 0.09^2)$ , width

$s_y \sim \mathcal{N}(0.3, 0.05^2)$ , and height  $s_z \sim \mathcal{N}(0.17, 0.03^2)$ . Since the details and code of the participating algorithms have not been publicly released by the organizers, we compare our method with continuous-domain packing algorithms introduced in Section 4.3. The test results are summarized in Table 14. In the continuous domain, our method continues to effectively utilize the operational properties of selectable and previewed items for efficient planning, with performance improving as decision variable available increases.

## C.4 Running Costs

For 3D-BPP of online needs, the running cost for placing each item is especially important. We count the running costs of the experiments in Section 4.1 and Section 4.3 and summarize them in Table 15. Each running cost at time step  $t$  is counted from putting down the previous item  $n_{t-1}$  until the current item  $n_t$  is placed, which includes the time to make placement decisions, the time to check placement feasibility, and the time to interact with the packing environment. The running cost of our method is comparable to most baselines. Our method can meet real-time packing requirements in both the discrete solution space and continuous solution space.

## C.5 Scalability

The number of PCT nodes changes constantly with the generation and removal of leaf nodes during the packing process. To verify whether our method can solve packing problems with a larger scale  $|\mathbf{B}|$ , we conduct a stress test on *setting 2* where the most orientations are allowed and the most leaf nodes are generated. We limit the maximum item sizes  $s^d$  to  $S^d/5$  so that more items can be accommodated. We transfer the best-performing policies on *setting 2* (trained with EMS) to these new datasets without any fine-tuning. The results are summarized in Table 16.

PCT size will not grow exponentially with packing scale  $|\mathbf{B}|$  since invalid leaf nodes will be removed from leaf nodes  $\mathbf{L}$  during the packing process, both discrete and continuous cases. For continuous cases,  $|\mathbf{L}|$  is more sensitive to  $|\mathbf{B}|$  due to the diversity of item sizes (i.e.  $|\mathcal{I}| = \infty$ ), however,  $|\mathbf{L}|$  still doesn't explode with  $|\mathbf{B}|$  and it grows in a sub-linear way. Our method can execute packing decisions at a real-time speed with controllable PCT sizes, even if the item scale is around two hundred.

## D Visualized Results

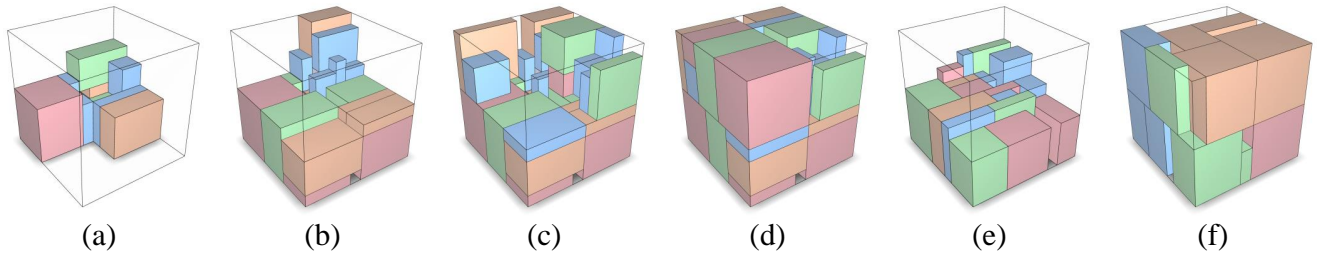
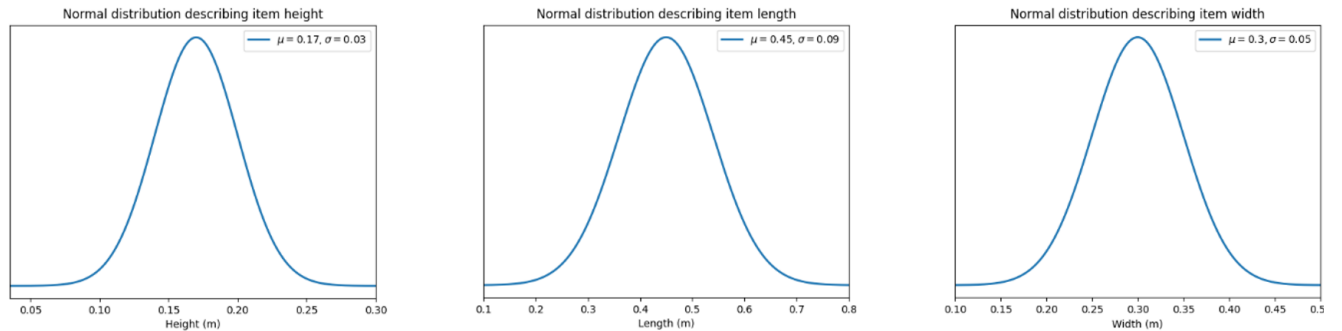
We visualize the experimental results of different BPP variations on three settings in Figure 23, Figure 24, and Figure 25. It is clearly observed that as the number of

**Table 12.** Transfer the best-performing PCT policies directly to the disturbed item sampling distributions. Dif. means how much the generalization performance drops from the undisturbed case ( $\delta_i = 0$ ).

Disturbance	Setting 1				Setting 2				Setting 3			
	Uti. $\uparrow$	Var. $\downarrow$	Num. $\uparrow$	Dif. $\downarrow$	Uti. $\uparrow$	Var. $\downarrow$	Num. $\uparrow$	Dif. $\downarrow$	Uti. $\uparrow$	Var. $\downarrow$	Num. $\uparrow$	Dif. $\downarrow$
$\delta_i = 0$	76.0%	4.2	29.4	0.0%	86.0%	1.9	33.0	0.0%	75.7%	4.6	29.2	0.0%
$\delta_i \in [-20\%, 20\%]$	75.6%	4.6	29.1	0.5%	85.7%	2.1	32.8	0.3%	75.3%	4.5	29.0	0.5%
$\delta_i \in [-40\%, 40\%]$	75.5%	4.5	29.0	0.7%	85.6%	2.1	32.8	0.5%	75.6%	4.8	29.3	0.1%
$\delta_i \in [-60\%, 60\%]$	75.5%	4.3	28.9	0.7%	85.8%	2.1	32.8	0.2%	75.5%	4.8	28.9	0.3%
$\delta_i \in [-80\%, 80\%]$	75.7%	4.5	29.2	0.4%	85.6%	2.2	32.9	0.5%	75.4%	4.9	29.3	0.4%
$\delta_i \in [-100\%, 100\%]$	75.8%	4.4	29.0	0.3%	85.5%	2.2	32.6	0.6%	75.3%	4.7	29.3	0.5%

**Table 13.** Generalization performance on unseen items. All policies are trained with the EV scheme.

Train	Test	Setting 1			Setting 2			Setting 3		
		Uti. $\uparrow$	Var. $\downarrow$	Num. $\uparrow$	Uti. $\uparrow$	Var. $\downarrow$	Num. $\uparrow$	Uti. $\uparrow$	Var. $\downarrow$	Num. $\uparrow$
$ \mathcal{I}  = 125$	$ \mathcal{I}  = 125$	76.0%	4.2	29.4	85.3%	2.1	32.8	75.7%	4.6	29.2
$ \mathcal{I}_{sub}  = 100$	$ \mathcal{I}_{sub}  = 100$	74.4%	5.1	29.4	86.3%	1.7	33.8	74.2%	4.7	29.3
$ \mathcal{I}_{sub}  = 100$	$ \mathcal{I}  = 125$	74.6%	5.4	28.9	85.6%	2.6	33.0	74.4%	5.2	28.8

**Figure 21.** (a)~(d) Different packing stages of the same sequence. The learned policies assign little items (colored in blue) to gaps and save room for future uncertainty. (e) Online 3D-BPP where load balancing is considered. (f) Online 3D-BPP with isle-friendliness, and different color means different item categories.**Figure 22.** Item dimensions of ICRA stacking challenge.**Table 14.** Performance comparisons on ICRA stacking challenge benchmark (Sim4Dexterity 2023).

Method	Prev.	Sel.	Un.	Setting 1				Setting 2				Setting 3			
				Uti. $\uparrow$	Var. $\downarrow$	Num. $\uparrow$	Gap $\downarrow$	Uti. $\uparrow$	Var. $\downarrow$	Num. $\uparrow$	Gap $\downarrow$	Uti. $\uparrow$	Var. $\downarrow$	Num. $\uparrow$	Gap $\downarrow$
BR	$p = 1$	$s = 1$	$u > 0$	53.4%	2.7	53.4	16.3%	61.6%	0.7	61.6	12.7%	53.7%	2.5	53.7	17.1%
OnlineBPH	$p = 1$	$s = 1$	$u > 0$	36.4%	12.5	36.4	42.9%	46.7%	1.3	46.8	33.9%	36.7%	12.7	36.8	43.4%
LSAH	$p = 1$	$s = 1$	$u > 0$	43.6%	11.7	43.6	31.7%	66.4%	0.6	66.4	5.9%	43.9%	11.9	43.9	32.3%
PCT	$p = 1$	$s = 1$	$u > 0$	<b>63.8%</b>	<b>1.5</b>	<b>63.6</b>	<b>0.0%</b>	<b>70.6%</b>	<b>0.3</b>	<b>70.5</b>	<b>0.0%</b>	<b>64.8%</b>	<b>2.1</b>	<b>64.7</b>	<b>0.0%</b>
ToP	$p = 10$	$s = 1$	$u > 0$	70.2%	0.4	70.8	–	72.9%	0.4	73.3	–	68.7%	1.3	69.1	–
ToP	$p = 10$	$s = 5$	$u > 0$	70.6%	0.5	71.2	–	74.3%	0.3	74.7	–	74.7%	0.4	74.9	–
ToP	$p = 10$	$s = 10$	$u > 0$	72.2%	0.2	72.5	–	76.2%	0.2	76.8	–	76.0%	0.3	77.0	–

packing decision variables increases, the packing results become more compact. We also provide the visualized results of large-scale packing in Figure 26. Each plot is

about result tested by a randomly generated item sequence. The real-world packing results conducted via industrial production are provided in Figure 27.

**Table 15.** Running costs (*seconds*) tested on online 3D-BPP with discrete solution space (Section 4.1) and continuous solution space (Section 4.3). The running costs of the latter are usually more expensive since checking Constraints 2 and 3 in the continuous domain is more time-consuming.

	Method	Setting 1		Setting 2		Setting 3	
		Discrete	Continuous	Discrete	Continuous	Discrete	Continuous
Heuristic	Random	$4.59 \times 10^{-2}$	—	$2.03 \times 10^{-2}$	—	$4.62 \times 10^{-2}$	—
	HM	$4.76 \times 10^{-2}$	—	$3.01 \times 10^{-2}$	—	$4.55 \times 10^{-2}$	—
	DBL	$5.58 \times 10^{-2}$	—	$1.87 \times 10^{-2}$	—	$5.44 \times 10^{-2}$	—
	BR	$1.50 \times 10^{-2}$	$1.69 \times 10^{-2}$	$1.74 \times 10^{-2}$	$1.76 \times 10^{-2}$	$1.42 \times 10^{-2}$	$1.62 \times 10^{-2}$
	OnlineBPH	$5.89 \times 10^{-3}$	$1.48 \times 10^{-2}$	$3.39 \times 10^{-3}$	$7.17 \times 10^{-3}$	$4.86 \times 10^{-3}$	$1.38 \times 10^{-2}$
	LSAH	$1.22 \times 10^{-2}$	$1.44 \times 10^{-2}$	$4.98 \times 10^{-3}$	$7.02 \times 10^{-3}$	$1.14 \times 10^{-2}$	$1.33 \times 10^{-2}$
	MACS	$2.68 \times 10^{-2}$	—	$3.00 \times 10^{-2}$	—	$2.79 \times 10^{-2}$	—
DRL	CDRL	$5.51 \times 10^{-2}$	—	$1.33 \times 10^{-2}$	—	$3.31 \times 10^{-2}$	—
	PCT & CP	$8.43 \times 10^{-3}$	$1.61 \times 10^{-2}$	$7.36 \times 10^{-3}$	$1.52 \times 10^{-2}$	$8.79 \times 10^{-3}$	$1.73 \times 10^{-2}$
	PCT & EP	$1.22 \times 10^{-2}$	$3.73 \times 10^{-2}$	$1.13 \times 10^{-2}$	$1.57 \times 10^{-2}$	$1.25 \times 10^{-2}$	$3.65 \times 10^{-2}$
	PCT & EMS	$1.77 \times 10^{-2}$	$4.11 \times 10^{-2}$	$9.49 \times 10^{-3}$	$2.36 \times 10^{-2}$	$1.80 \times 10^{-2}$	$3.08 \times 10^{-2}$
	PCT & EV	$2.66 \times 10^{-2}$	$4.46 \times 10^{-2}$	$1.25 \times 10^{-2}$	$3.21 \times 10^{-2}$	$2.61 \times 10^{-2}$	$4.38 \times 10^{-2}$

**Table 16.** Scalability on larger packing problems.  $|L|$  is the average number of leaf nodes per step. Run. is the running cost.  $|L|$  will not increase exponentially with  $|B|$  since invalid leaf nodes will be removed.

Item sizes	$ B $	$ L $	Discrete			$ L / B $	$ B $	$ L $	Continuous		
			Uti.	Run.					Uti.	Run.	$ L / B $
$[S^d/10, S^d/2]$	33.0	51.5	86.0%	$9.5 \times 10^{-2}$	1.6		27.0	197.5	66.3%	$2.4 \times 10^{-2}$	7.3
$[S^d/10, S^d/5]$	241.3	67.2	81.3%	$9.8 \times 10^{-3}$	0.3		185.4	956.5	61.9%	$3.7 \times 10^{-2}$	5.2

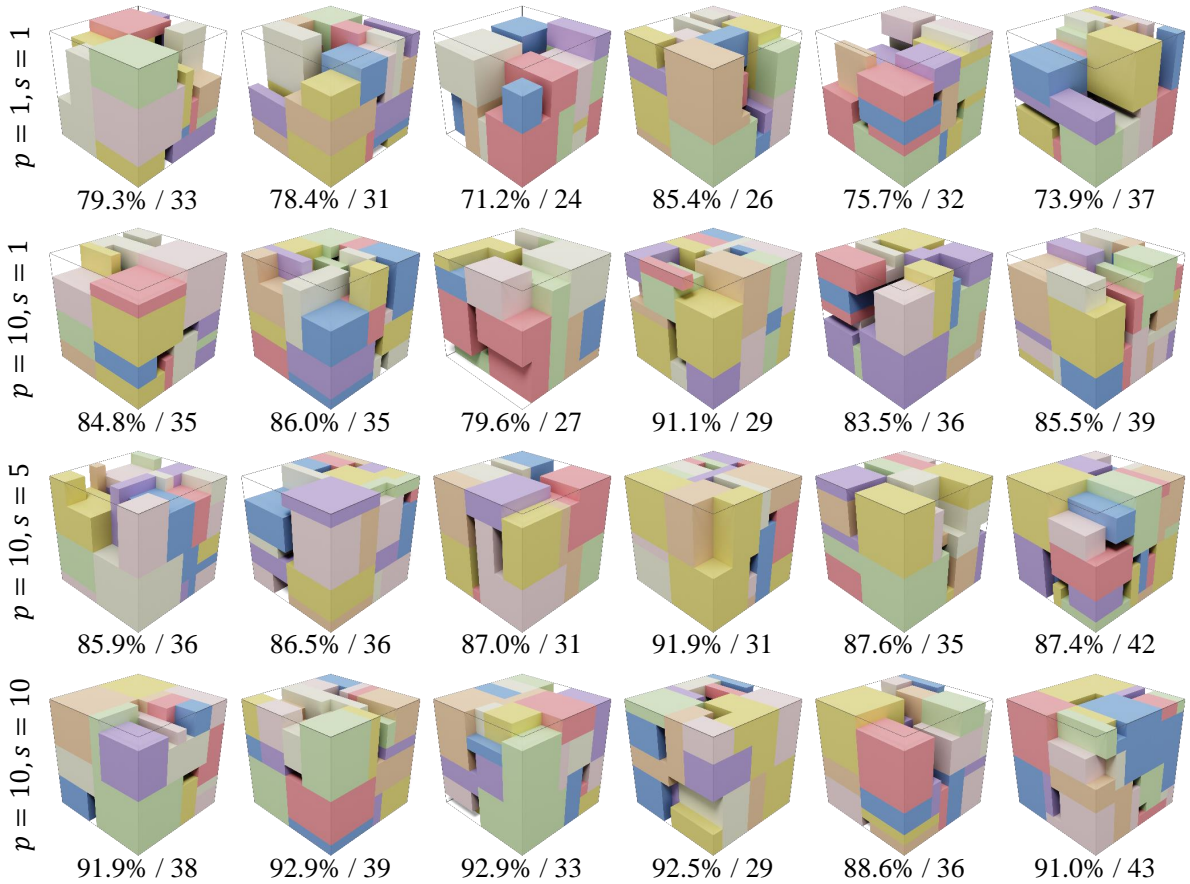


**Figure 23.** Visualized results of different BPP variations on setting 1, with space utilization and packed item number labeled below. Each column corresponds to the same test data.



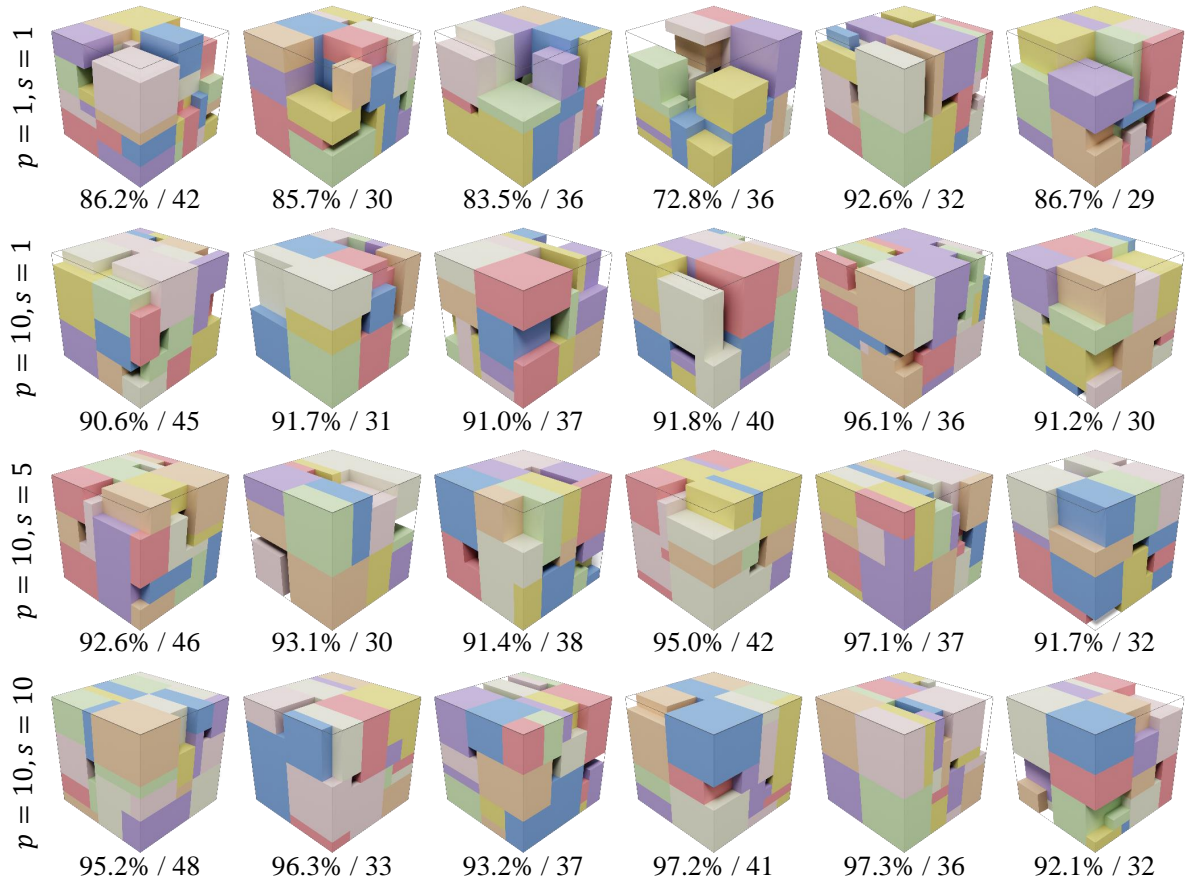


**Figure 24.** Visualized results of different BPP variations on setting 2. Each column corresponds to the same test data.

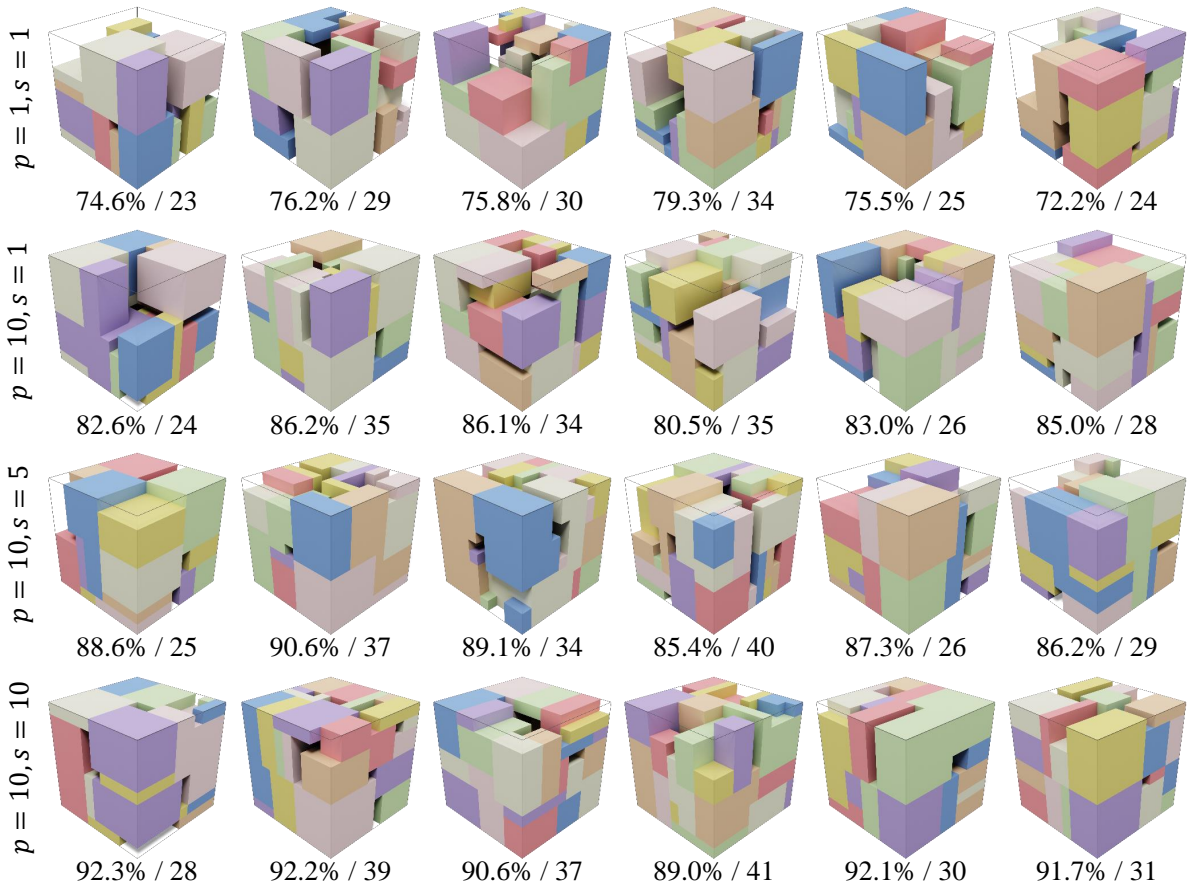


**Figure 25.** Visualized results of different BPP variations on setting 3. Each column corresponds to the same test data.



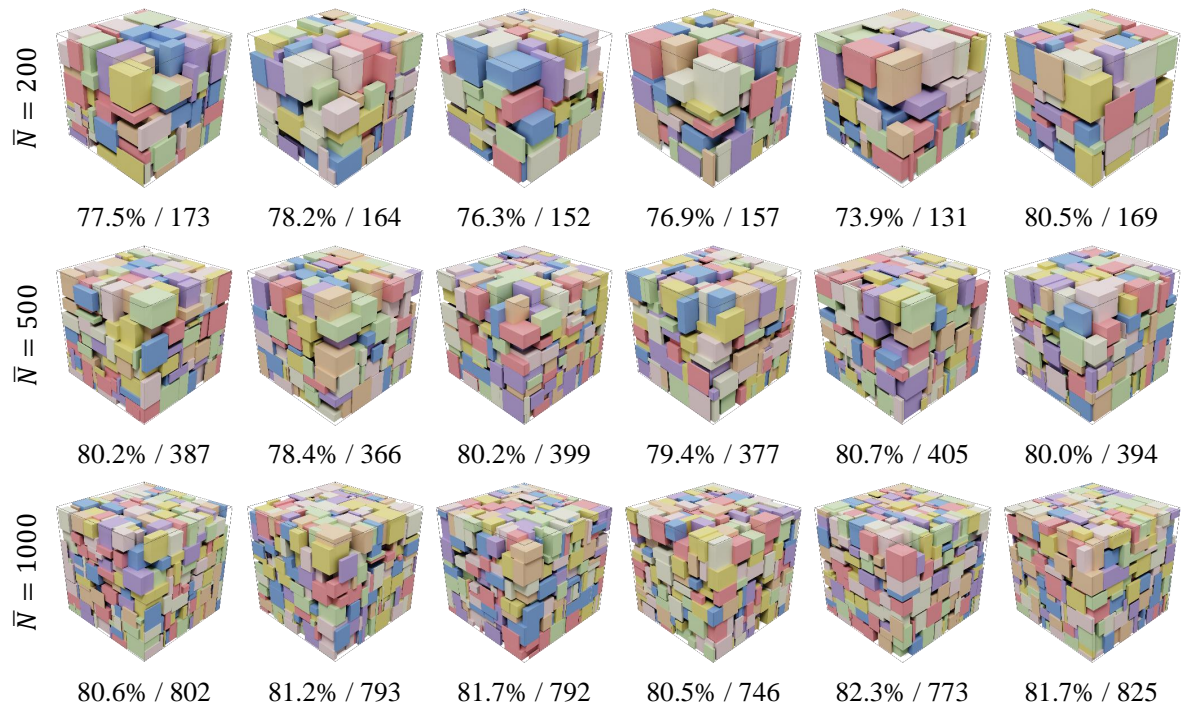


**Figure 26.** Visualized results of large-scale packing at various problem scales, with space utilization and item number labeled.

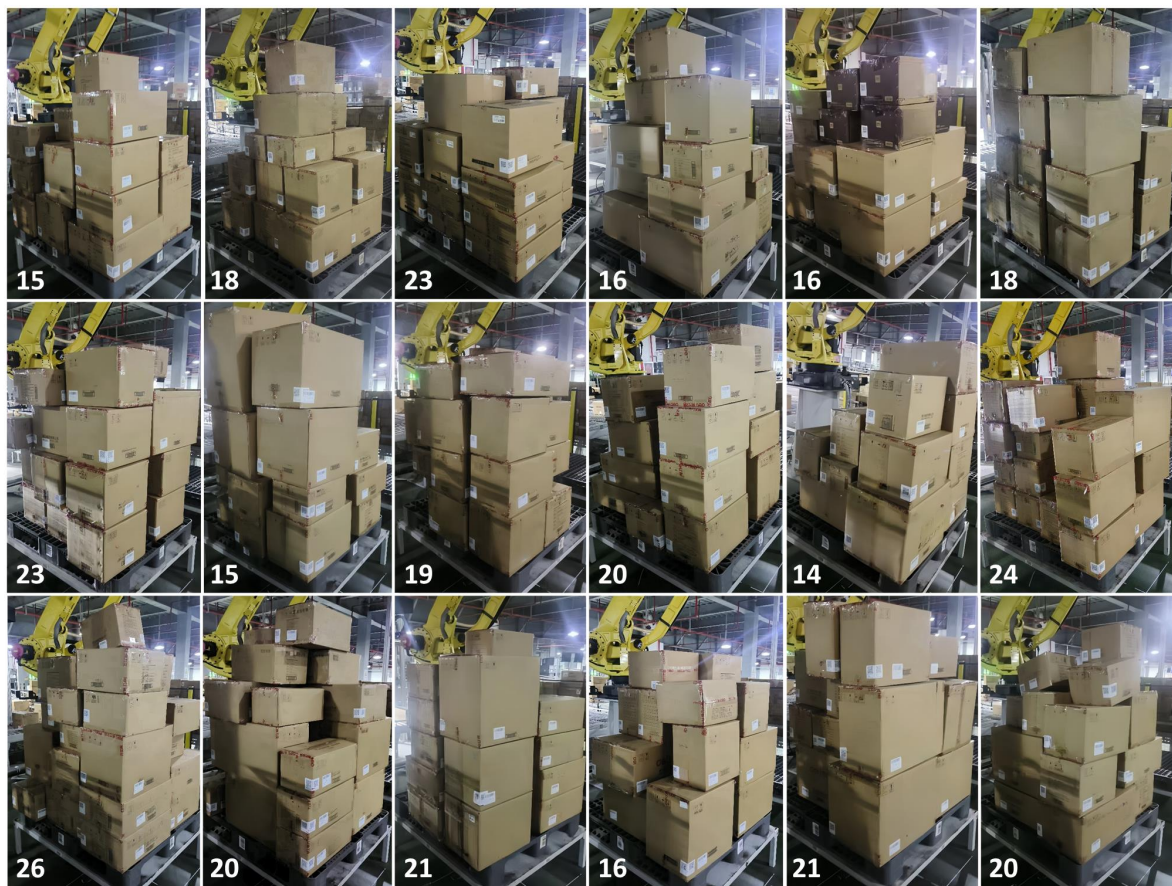


**Figure 27.** Real-world packing results. The number of packed items on each pallet is labeled in the bottom left corner.